Nuclear basket proteins Mlp1 and Nup2 drive heat shock-induced 3D genome restructuring

Suman Mohajan, Linda S. Rubio, David S. Gross*
Department of Biochemistry and Molecular Biology
Louisiana State University Health Sciences Center
Shreveport, LA 71130

*Corresponding author: david.gross@lsuhs.edu

Keywords: Nuclear Pore Complex; Heat Shock Response; Nup1; Nup145; Heat Shock Factor (Hsf1); chromatin; RNA Pol II; transcriptional condensates; *Saccharomyces cerevisiae*

Short running title: The yeast NPC drives 3D genome restructuring

ABSTRACT

The nuclear pore complex (NPC), a multisubunit complex located within the nuclear envelope, regulates RNA export and the import and export of proteins. Here we address the role of the NPC in driving thermal stress-induced 3D genome repositioning of *Heat Shock Responsive* (*HSR*) genes in yeast. We found that two nuclear basket proteins, Mlp1 and Nup2, although dispensable for NPC integrity, are required for driving *HSR* genes into coalesced chromatin clusters, consistent with their strong, heat shock-dependent recruitment to *HSR* gene regulatory and coding regions. *HSR* gene clustering occurs predominantly within the nucleoplasm and is independent of the essential scaffold-associated proteins Nup1 and Nup145. Notably, double depletion of Mlp1 and Nup2 has little effect on the formation of Heat Shock Factor 1 (Hsf1)-containing transcriptional condensates, Hsf1 and Pol II recruitment to *HSR* genes, or *HSR* mRNA abundance. Our results define a 3D genome restructuring role for nuclear basket proteins extrinsic to the NPC and downstream of *HSR* gene activation.

Introduction

The complex three-dimensional (3D) architecture of eukaryotic chromatin is established and maintained through intricate looping and folding interactions. These interactions bring into close proximity enhancers and promoters (that may be tens or hundreds of kilobases apart) as well as promoters and terminators (O'Sullivan et al., 2004; Ansari and Hampsey, 2005; Levine et al., 2014; Dekker and Mirny, 2016). In addition to these local looping and folding interactions, chromosomal loci can undergo dynamic repositioning within the nucleus. Such restructuring of 3D chromatin architecture has been suggested to regulate gene expression, replication, DNA repair, chromosomal transposition and mRNA export (Casolari et al., 2004; Pliss et al., 2009; Feuerborn and Cook, 2015; Scholz et al., 2019; Miné-Hattab and Chiolo, 2020; Babokhov et al., 2020). However, the underlying molecular mechanisms by which 3D genome structural changes occur and how these topological alterations impact nuclear processes remain unclear.

Dynamic aspects of 3D chromatin architecture can be investigated using a powerful heat shock-responsive system established in the budding yeast *Saccharomyces cerevisiae*. The heat shock response (HSR) is an evolutionarily conserved, adaptive mechanism that is used by eukaryotic organisms to maintain protein homeostasis in response to thermal, chemical and oxidative stress (reviewed in Verghese et al., 2012; Fujimoto et al., 2023). It is characterized by the transcriptional upregulation of genes encoding heat shock proteins (HSPs) and other homeostasis factors (reviewed in Verghese et al., 2012; Gomez-Pastor et al., 2018). This transcriptional response strictly depends on a sequence-specific transcription factor (TF), Heat Shock Factor 1 (Hsf1), that inducibly binds its cognate heat shock elements (HSEs) situated upstream of *HSR* genes (Sorger and Nelson, 1989; Hentze et al., 2016; Pincus et al., 2018). We have observed that in response to acute heat shock, Hsf1 forms subnuclear clusters that have characteristics of transcriptional condensates and contain Hsf1, RNA Pol II, and Mediator (Chowdhary et al., 2019, 2022). These condensates drive robust cis- and trans-intergenic interactions between *HSR* genes (Chowdhary et al., 2022) that culminate in their coalescence into intranuclear foci (*HSR*

gene coalescence [HGC]). While Hsf1, the large subunit of Pol II (Rpb1) and the Mediator Tail subunit Med15 contribute to HGC (Chowdhary et al., 2019, 2022; Rubio et al., 2024; Male et al., unpubl. observations), the potential role of other nuclear factors remains largely unexplored.

It has been previously observed that inducible genes in yeast spatially reposition from the nuclear interior to its periphery upon their activation (Brickner and Walter, 2004; Casolari et al., 2004; Dieppois et al., 2006; Ahmed et al., 2010; Taddei et al., 2010; Brickner et al., 2016; Dultz et al., 2016; Brickner et al., 2019; Li et al., 2024). Such repositioning appears to be mediated by the interaction between the genes and the nuclear pore complex (NPC) (Brickner and Brickner, 2012; Brickner et al., 2015; Randise-Hinchliff and Brickner, 2016), a conserved multiprotein assembly located at the surface of the nucleus. The NPC is comprised of multiple copies of ~30 different proteins (nucleoporins (Nups)) which regulate RNA export as well as the import and export of proteins across the nuclear envelope. Nups are either stably or dynamically associated with the core NPC and nuclear basket (reviewed in Beck et al., 2004; Hampoelz et al., 2019; Akey et al., 2022; Zsok et al., 2024).

The NPC scaffold is composed of Y complexes that pass through the center of the NPC (Akey et al., 2022; Singh et al., 2024) and maintain NPC integrity. Nup145 (ortholog of human Nup98) is an essential nucleoporin of the Y complex that plays a critical role in maintaining the integrity of the NPC (Wente and Blobel, 1994; Teixeira et al., 1997; Palancade et al., 2007). It undergoes autoproteolytic cleavage and generates two functionally distinct polypeptides, Nup145C and Nup145N. Nup145C integrates into the Y complex, acts as a scaffold, and is slowly exchanging, while Nup145N becomes a part of the central core, is more dynamic, and interacts with numerous active transport processes (Hakhverdyan et al., 2021). In addition, Nup145 has been suggested to associate with chromatin and assist in the repositioning of an activated gene to the NPC (Sarma et al., 2007).

The nuclear basket (NB) consists of FG or FXF(G) domain-containing Nups (Nup1, Nup2, and Nup60) and coiled-coil domain-containing Nups (Mlp1 and Mlp2) (Strambio-de-Castillia et al., 1999; Dilworth et al., 2001; Niepel et al., 2013; Lin and Hoelz, 2019; Hakhverdyan et al., 2021; Singh et al., 2024). While Nup1 is scaffold-associated and connects the basket with the nuclear membrane (Mészáros et al., 2015; Singh et al., 2024), the filamentous Mlps extend toward the nucleoplasm and converge into a distal ring (Strambio-de-Castillia et al., 1999; Kosova et al., 2000; Niepel et al., 2013; Akey et al., 2022; Singh et al., 2024) (schematically depicted in **Figure 1A**). It has been suggested that the nuclear basket regulates membrane curvature and NPC integrity, distribution, and mobility (Niepel et al., 2013; Mészáros et al., 2015; Zsok et al., 2024). Additionally, the NB serves as a docking site for mRNP granules, facilitating mRNA quality control and efficient export (Dieppois and Stutz, 2010). In addition to its canonical transport function, the nuclear basket is also involved in DNA repair, transcriptional regulation and gene targeting (reviewed in Palancade et al., 2007; Sood and Brickner, 2014; Freudenreich and Su, 2016). Yet how the nuclear basket regulates the abovementioned processes remains poorly understood. Key roles of Nup145 and the nuclear basket Nups are summarized in Table 1.

The NPC has been implicated in regulating transcription in yeast (Brickner and Walter, 2004; Taddei et al., 2006; Brickner et al., 2007); likewise, NPC proteins have been found associated with mammalian enhancers and super-enhancers (SEs) (Ibarra et al., 2016; Scholz et al., 2019; Ahn et al., 2021; Zhu et al., 2022; Tyagi et al., 2023). It has been suggested that certain nucleoporins can undergo phase separation that may facilitate the formation of transcriptional hubs (Tyagi et al., 2023). Such hubs then concentrate chromatin structural proteins and transcriptional coactivators at the SEs that may facilitate transcription or mRNA export or both. Coalescence of *HSR* genes in yeast bears important similarities to mammalian super-enhancers, including the presence of extensive DNA loops and transcriptional condensates that concentrate chromatin-associated TFs and transcriptional machinery and co-activators (Kainth et al., 2021; Chowdhary et al., 2022). Here, we provide evidence that *HSR* genes reposition to the NPC in response to heat stress and show that *HSR* genes can coalesce at the pore and (more frequently) within the nucleoplasm. While the essential scaffold protein

Nup145 and scaffold-associated nuclear basket protein Nup1 play no detectable role in *HSR* gene coalescence, the dynamically exchangeable nuclear basket proteins Mlp1 and Nup2 play a critical role, and likely do so in their NPC-free state.

Results

Coalescence of *Heat Shock Response* genes preferentially occurs within the nucleoplasm

Previous studies have suggested that a variety of inducible genes in *S. cerevisiae,* including those that respond to stress, relocate from the nuclear interior to the nuclear periphery upon their transcriptional activation as discussed above. Certain of these genes have a Gene Recruitment Sequence (GRS) within their upstream regions that is implicated in such repositioning (Brickner and Brickner, 2012; Brickner et al., 2015, 2016; Randise-Hinchliff and Brickner, 2016). However, the underlying molecular mechanisms remain largely unknown. We have previously reported that Hsf1-regulated *HSR* genes, dispersed across multiple chromosomes, physically interact and cluster together within minutes following cell exposure to proteotoxic stresses such as heat shock or ethanol stress (Chowdhary et al., 2017, 2019, 2022; Rubio et al., 2024).

To address whether such coalescence occurs at the nuclear pore or within the nucleoplasm, we constructed a strain in which the nuclear pore transmembrane protein Pom34 was labeled with mCherry and the *HSP104* and *HSP12* genes were tagged with LacO arrays to which LacI-GFP was bound (schematically summarized in **Figure 1B**). We then conducted live imaging of cells subjected to an instantaneous HS (25°C to 38°C) and examined coalescence of the two genes following 2.5 and 10 min of HS. As shown in **Figure 1C**, coalescence occurred at both the nuclear pore and within the nucleoplasm. Overall, of the cells that exhibited *HSP12-HSP104* coalescence (~30% of the total), coalescence at the periphery was observed in less than one-third, while coalescence within the nucleoplasm was observed in greater than two-thirds (**Figure 1D)**. Fixed cell microscopy similarly revealed examples of HS-induced *HSP12-HSP104* coalescence at the nuclear periphery as well as within the nuclear interior (A.S. Kainth, personal communication). These data indicate that *HSR* gene coalescence can occur within the nucleoplasm, and it is likely the preferred location.

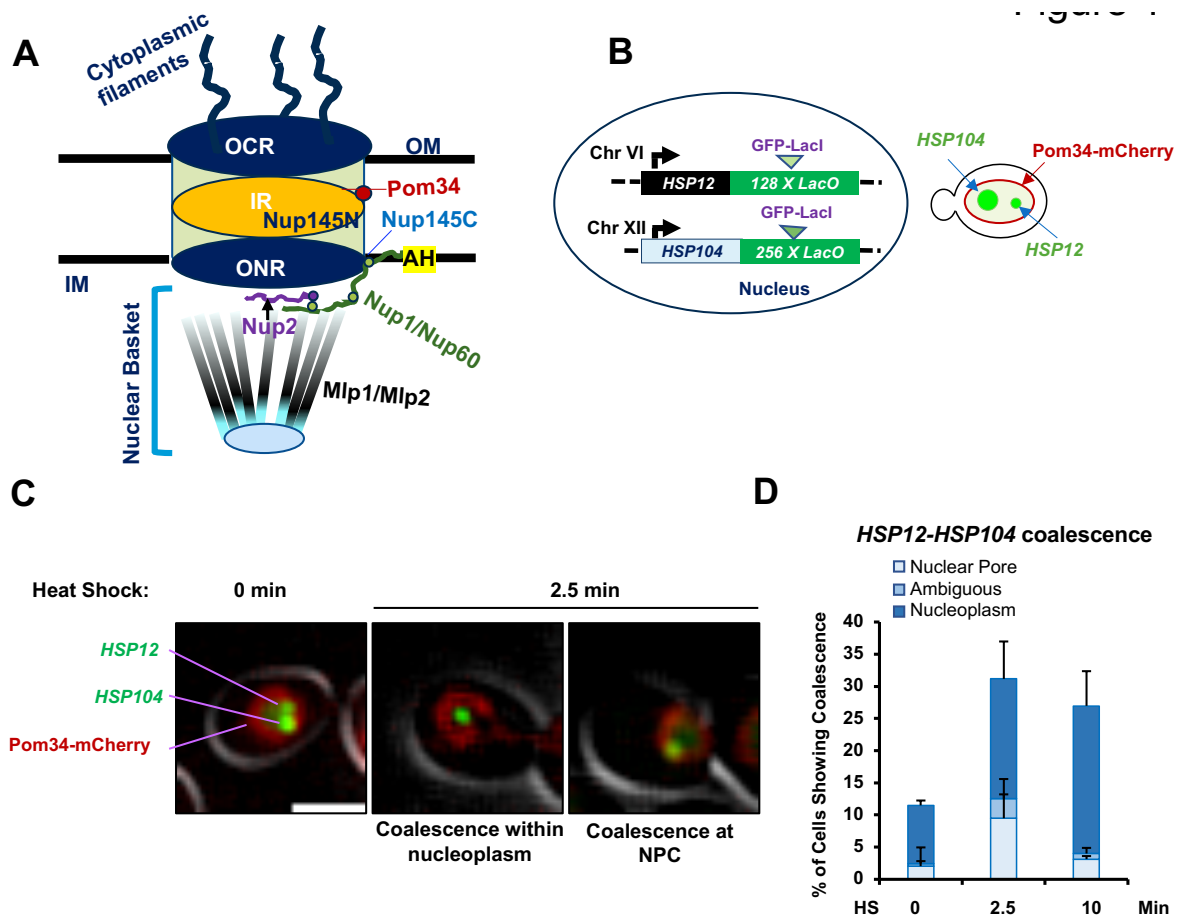

Figure 1. *HSR* gene coalescence occurs both within the nuclear interior and at the nuclear pore complex.

A. The yeast NPC. IM, Inner membrane; OM, Outer membrane; OCR, Outer Cytoplasmic Ring; IR, Inner Ring; ONR, Outer Nuclear Ring; AH, Amphipathic helix; Nup145C, C-terminal domain of Nup145; Nup145N, N-terminal domain of Nup145. Each Nup exists in multiple copies; only one representative copy is shown.

B. Schematic depiction of the LacI-GFP tagged heterozygous diploid strain ASK706 bearing one copy each of *HSP104-lacO*$_{256}$ and *HSP12-lacO*$_{128}$ and expressing the mCherry-marked nuclear pore transmembrane protein Pom34.

C. Coalesced *HSP104* and *HSP12* gene foci are found at the NPC and within the nucleoplasm. Cells were imaged both prior to and following a 25° to 38°C heat shock (HS). Two examples of 2.5 min HS, with different localization for the coalesced foci, are depicted. Scale bar: 2 µm.

D. Quantification of *HSP104-HSP12* localization data, scored using the nuclear pore marker Pom34-mCherry, in cells treated as in C. On average, 100 cells were scored per sample. N=2. Error bars represent standard deviation.

Nup1 and Nup145 are important for maintaining integrity of the NPC but play no detectable role in heat shock-induced *HSR* gene coalescence

As discussed above, certain NPC proteins have been implicated in the repositioning of inducible genes to the nuclear pore upon their activation. To address whether the NPC is required to drive the coalescence of *HSR* genes, we initially tested the involvement of two essential, scaffold-associated nucleoporins, Nup1 and Nup145. To do so, we conditionally depleted these proteins using the Auxin Inducible Degradation (AID) technique (Nishimura et al., 2009). Both proteins have been reported to maintain integrity of the NPC and nuclear envelope (Palancade et al., 2007; Wente and Blobel, 1994; Mészáros et al., 2015). They also have been implicated in repositioning activated genes to the nuclear pore (Cabal et al., 2006; Brickner and Brickner, 2010; Brickner et al., 2016; Sarma et al., 2007). We tagged each gene with a mini-degron **(Figure 2A)** and as shown in **Figure 2B**, 85 - 95% degradation of each protein was achieved within 60 min of adding auxin.

To examine the effect of simultaneous depletion of Nup1 and Nup145 on NPC integrity, we performed imaging of live cells expressing mCherry-labeled Pom34 **(Figures 2C, 2D),** a protein associated with the NPC inner ring (Akey et al., 2022). NPC integrity was compromised upon double depletion of Nup1 and Nup145, as ~75% of cells harbored at least one Pom34 punctate structure **(Figure 2D, 2E).** Note that addition of auxin alone did not affect NPC integrity, while the degron tag itself had some impact. This observation is consistent with previous studies that found a mutation in either N-terminal or C-terminal domains of Nup145 compromised NPC structure (Wente and Blobel, 1994; Dockendorff et al., 1997; Fernandez-Martinez et al., 2012). We additionally tested the effect of simultaneously depleting Nup1 and Nup145 on the integrity of the nuclear basket. Consistent with its effect on Pom34, double deletion of Nup1 and Nup145 disrupted the subnuclear localization of both Nup2-mNeonGreen (mNG) and Mlp1-mNG, leading to the formation of punctate structures **(Figure 2F).**

Figure 2

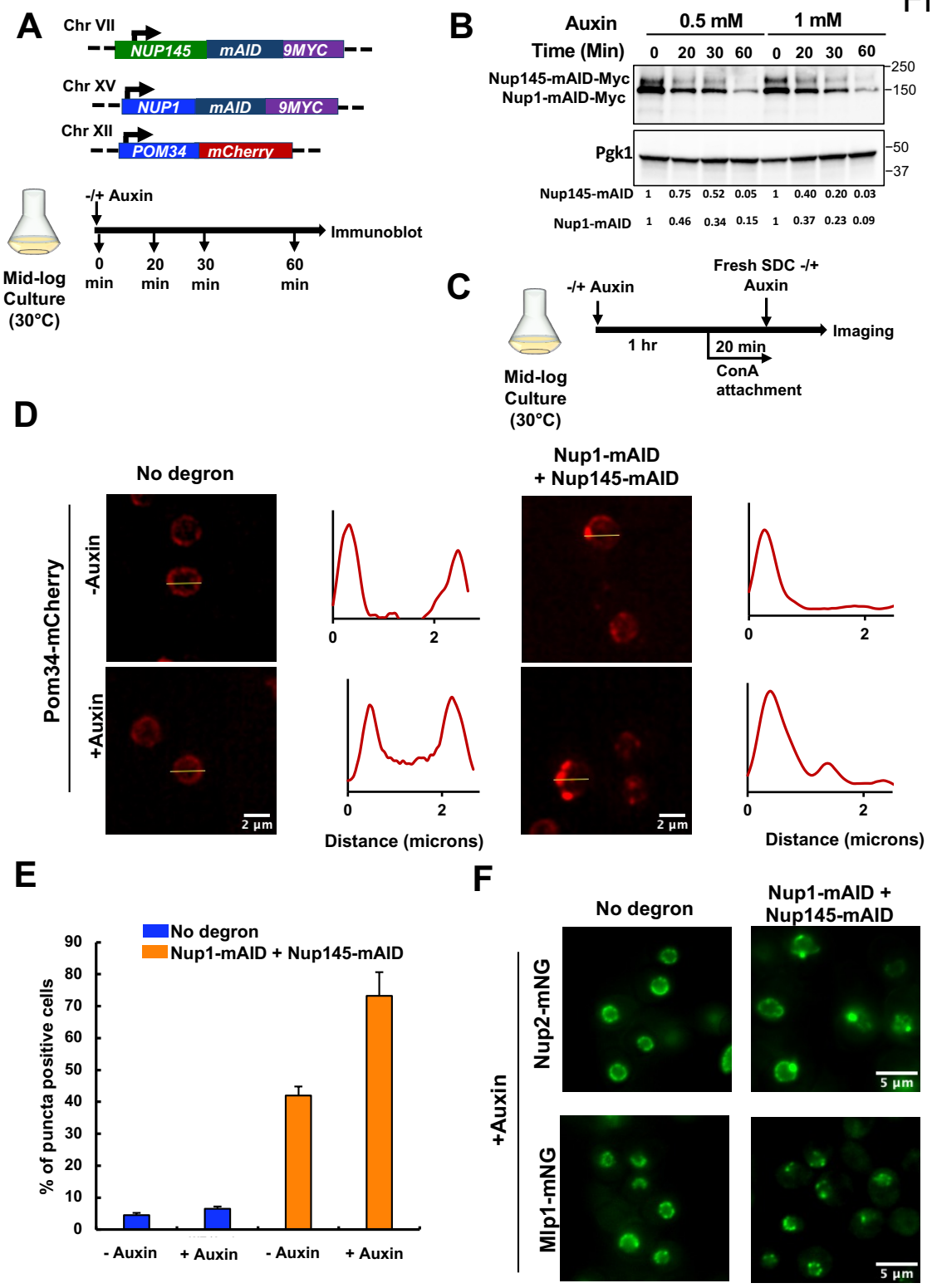
A
Chr VII
NUP145
mAID
9MYC
Chr XV
NUP1
mAID
9MYC
Chr XII
POM34
mCherry
-/+ Auxin
Immunoblot
0 min
20 min
30 min
60 min
Mid-log Culture (30°C)
B
Auxin
0.5 mM
1 mM
Time (Min)
0 20 30 60 0 20 30 60
Nup145-mAID-Myc
Nup1-mAID-Myc
250
150
Pgk1
50
37
Nup145-mAID 1 0.75 0.52 0.05 1 0.40 0.20 0.03
Nup1-mAID 1 0.46 0.34 0.15 1 0.37 0.23 0.09
C
-/+ Auxin
Fresh SDC -/+ Auxin
Imaging
1 hr
20 min
ConA attachment
Mid-log Culture (30°C)
D
No degron
Nup1-mAID + Nup145-mAID
Pom34-mCherry
-Auxin
+Auxin
2 µm
0
2
Distance (microns)
E
No degron
Nup1-mAID + Nup145-mAID
% of puncta positive cells
90
80
70
60
50
40
30
20
10
0
- Auxin
+ Auxin
- Auxin
+ Auxin
F
No degron
Nup1-mAID + Nup145-mAID
+Auxin
Nup2-mNG
Mlp1-mNG
5 µm

Figure 2. Simultaneous depletion of Nup1 and Nup145 perturbs NPC integrity and alters the distribution of Nup2 and Mlp1.

(A) Top: Relevant genotype of haploid strain SMY163 bearing *NUP145-mAID-9MYC*, *NUP1-mAID-9MYC* and *POM34-mCherry.* Bottom: Experimental strategy for optimizing auxin concentration and incubation time for double degradation.
(B) Immunoblot analysis of Nup1-mAID-9Myc and Nup145-mAID-9Myc in cells treated with different concentrations of indoleacetic acid (IAA) for the indicated times. Monoclonal antibody 9E10 was used to detect the levels of the respective proteins. Endogenous Pgk1 was used as a loading control.
(C) Experimental strategy for assessing NPC integrity upon simultaneous depletion of Nup1 and Nup145. Cells expressing mCherry-tagged Pom34 bearing either no degron (SMY160) or the Nup1-, Nup145- double degron (SMY163) were pretreated with 1 mM IAA or vehicle alone (0.17% ethanol) for 60 minutes at 30°C, followed by attachment to a ConA-coated VAHEAT substrate. Imaging was done using fluorescence spinning disk confocal microscopy (see Methods).
(D) Subnuclear localization of mCherry-tagged Pom34 in cells treated (or not) with 1 mM IAA. A representative maximum projection image (21 z-planes with a step size of 0.3 microns) of each treatment is shown. The intensity profile plot for each representative image is displayed on the right side of the respective image.
(E) Quantification of cells showing NPC punctate structure at the nuclear periphery in the indicated strains. Depicted values are means + SD, N=2. 100 cells per biological sample were analyzed.
(F) Subcellular localization of Nup2-mNG and Mlp1-mNG in no degron strains (SMY192 and SMY216) and double degron strains (SMY196 and SMY221) maintained at 25°C and treated with 1 mM IAA for ~60 min prior to imaging. A representative single z-plane is shown for each sample (step size of 0.5 microns).

To investigate the effect of Nup1-, Nup145-double depletion on the physical clustering of *HSR* genes (*HSR* gene coalescence), we used a powerful crosslinking, digestion and proximity ligation-based technique (Taq I - 3C) (Chowdhary et al., 2020; Rubio et al., 2024). Cells were treated with auxin and then subjected to an acute HS as above. 3C analysis of the parental strain (lacking a degron-tagged gene) revealed a dramatic heat shock-dependent increase in both *cis*- and *trans*- intergenic interactions between *HSR* genes as previously observed (Chowdhary et al., 2017, 2019, 2022; Rubio & Gross, 2023; Rubio et al., 2024). (See **Figure S1** for *HSR* gene physical maps.) Note that there was almost no detectable 3C signal observed in non-stressed (0 min HS) cells **(Figures 3A** and **3B).** Notably, double depletion of Nup1 and Nup145 had little or no impact on the HS-induced interactions **(Figure 3A, 3B**; compare orange vs. blue bars**).** Collectively, these results indicate that while Nup1 and Nup145 are important for maintaining NPC integrity and the wild-type distribution of nuclear basket proteins, they play little or no role in driving the 3D restructuring of *HSR* genes in acutely heat-shocked cells.

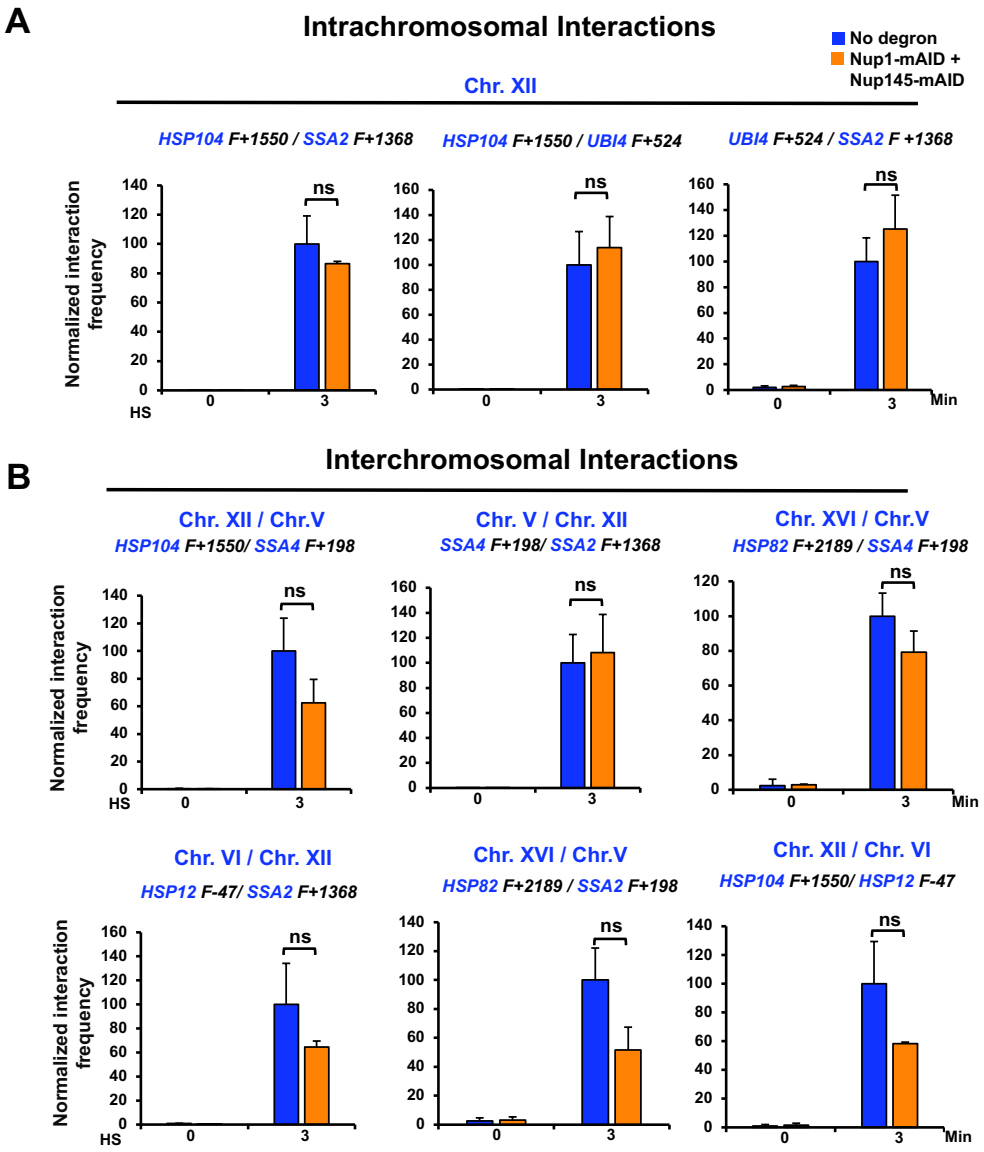

Figure 3. Nup1-, Nup145-double depletion has minimal effect on heat shock-induced 3D restructuring of *HSR* genes.

(A) Frequency of *cis*-interactions between the indicated Hsf1-regulated genes as detected by Taq I-3C. No degron (LRY016) and double degron (SMY148)-tagged cells were pretreated with 1 mM IAA for 60 min at 30°C prior to exposing them (or not) to HS (39°C). For the 0 min time point (NHS), cells were maintained at 25°C for ~10 min prior to crosslinking. For the HS samples, cells were similarly maintained at 25°C prior to initiating HS treatment. Loci examined in this study are illustrated in Suppl. Figure S1. Pairwise tests used forward (F; sense strand identical) primers positioned nearby the indicated Taq I site. Interaction frequencies were normalized with respect to the control strain, which was arbitrarily assigned 100. Shown are means + SD, N=2, qPCR=4. To determine significance, an unpaired two-tailed t-test was performed. ns, not significant (*p>0.05*).

(B) As in A, except *trans*-interactions were assayed.

Nup2 and Mlp1 are critically required to drive *HSR* genes into coalesced chromatin clusters

Next, given their reported role in targeting transcriptionally active genes to the NPC, we wished to investigate what role, if any, the nuclear basket proteins Nup2 and Mlp1 have in driving *HSR* gene coalescence. To address this, we performed live cell imaging of fluorophore-tagged genes and quantitative 3C of untagged and degron-tagged strains. For live cell imaging, we used heterozygous diploids that harbored single alleles of LacI-GFP marked *HSP104-lacO*$_{256}$ on Chr. XII and tetR-mCherry marked *HSP82-tetO*$_{200}$ on Chr. XVI and bore homozygous deletions of either *MLP1* or *NUP2* **(Figure S2A).** While chronic exposure to elevated temperature caused a fitness defect in either *nup2Δ / nup2Δ* or *mlp1Δ / mlp1Δ* cells, brief exposure had no effect on cell viability **(Figures S3A** and **S3B).** The cells were subjected to instantaneous HS (38°C) for various durations (0, 2.5, 10, and 17.5 min), and images were captured using widefield fluorescence microscopy. As shown in **Figure S2B**, deletion of either *NUP2* or *MLP1* had only a mild effect on *HSP104* - *HSP82* gene coalescence.

As an orthogonal approach, we constructed Nup2-mAID and Mlp1-mAID expressing strains **(Figure 4A)** and performed 3C. 90 to 95% degradation of degron-tagged Nup2 and Mlp1 was achieved following addition of auxin for 30 min **(Figures 4B**, **4C**). As shown in **Figure S2C**, depletion of either Nup2 or Mlp1 had a moderate effect on both long-range *cis* (intrachromosomal) and *trans* (interchromosomal) *HSR* intergenic interactions, consistent with the above microscopic analysis. We additionally tested the role of each NB protein on HS-induced intragenic interactions. In previous work, we observed that transcriptionally activated *HSR* genes not only engage in intergenic interactions but also engage in intragenic looping between enhancer-promoter (E-P), promoter - coding region, and promoter - 3'-UTR (Chowdhary et al., 2017, 2019, 2022; Rubio et al., 2024). Depletion of either Nup2 or Mlp1 had only a modest effect on such interactions **(Figure S2D).** These results therefore suggest that Nup2 and Mlp1 individually have only a modest non-redundant role in driving either the spatial repositioning or intragenic restructuring of *HSR* genes in response to heat shock.

Given that the nuclear basket regulates the distribution and mobility of the NPC (Zsok et al., 2024) as well as NPC and nuclear envelope integrity (Mészáros et al., 2015), we wondered if together, Nup2 and Mlp1 might play a more substantial role in maintaining either NPC integrity or in governing 3D genome topology in heat-shocked cells. To address this, we performed a conditional double depletion of Nup2 and Mlp1 using the AID strategy as above and initially investigated its effect on NPC integrity by examining subnuclear localization of mCherry-tagged Pom34 **(Figures 4A, 4D).** Live cell imaging revealed that Pom34 perinuclear localization remained unaffected **(Figure 4E),** consistent with the notion that Nup2 and Mlp1 are not critical for NPC integrity.

To address the combined impact of Nup2 and Mlp1 on 3D genome architecture, we performed quantitative 3C on HS-induced no-degron and double-degron cells that had been previously exposed to auxin as above. As shown in **Figures 4F** and **4G**, simultaneous depletion of Nup2 and Mlp1 substantially reduced both intra-chromosomal and inter-chromosomal interactions between *HSR* genes. The combined depletion of Nup2 and Mlp1 not only impaired long-range intergenic interactions but also short-range intra-locus interactions, including those between enhancer - promoter, promoter - coding region, and promoter - 3'-UTR **(Figures 4H** and **S4).** Notably, double depletion of Nup2 and Mlp1 had minimal effect on the viability of acutely heat-shocked cells **(Figure S3C).** Altogether, these results indicate that the dynamic nuclear basket proteins are dispensable for maintaining NPC integrity, yet they have important, partially redundant roles in driving the heat shock-dependent 3D reorganization of *HSR* genes.

Figure 4

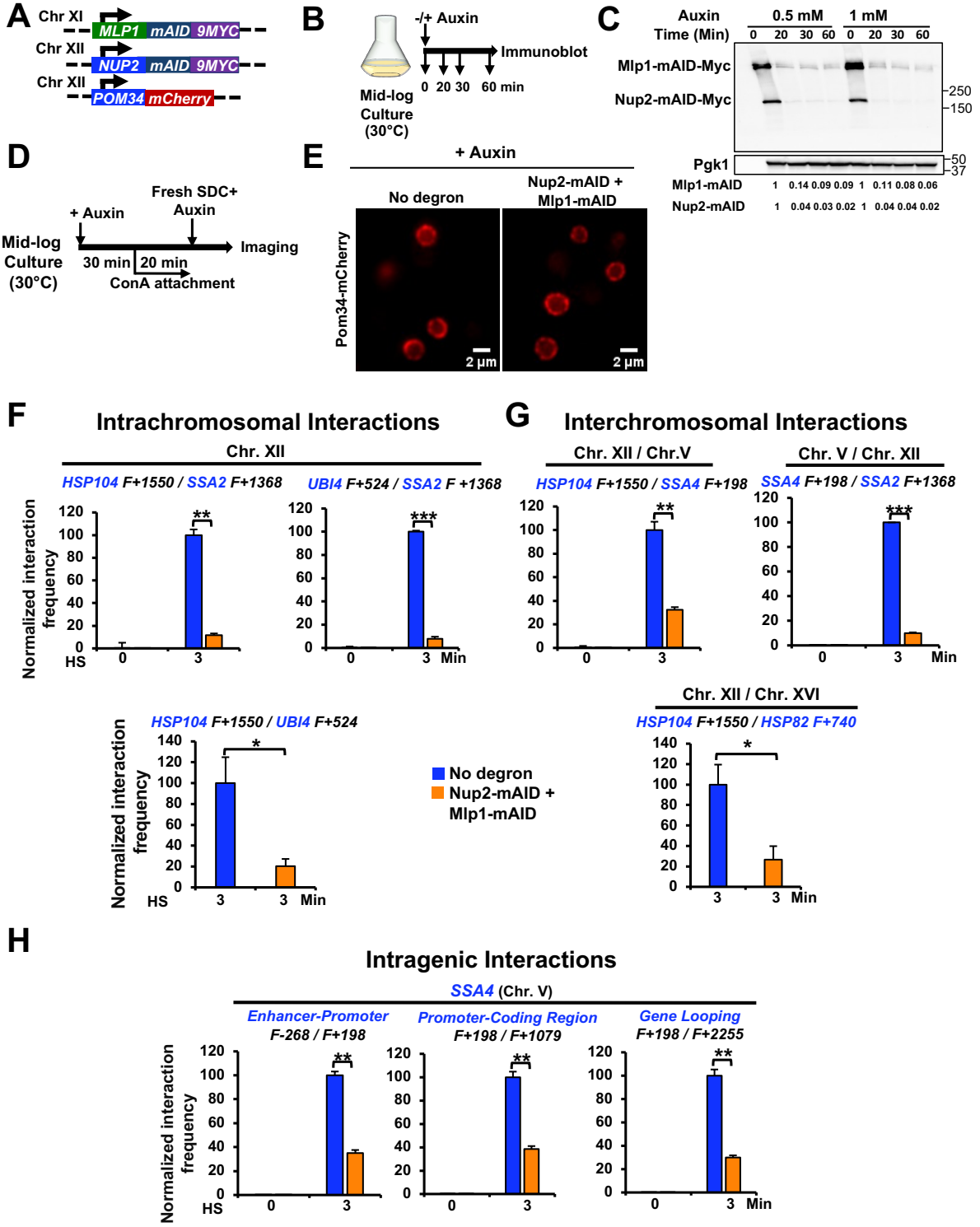
A
Chr XI
MLP1 mAID 9MYC
Chr XII
NUP2 mAID 9MYC
Chr XII
POM34 mCherry
B
-/+ Auxin
Immunoblot
0 20 30 60 min
Mid-log Culture (30°C)
C
Auxin
Time (Min)
0.5 mM
1 mM
0 20 30 60 0 20 30 60
Mlp1-mAID-Myc
Nup2-mAID-Myc
250
150
Pgk1
50
37
Mlp1-mAID 1 0.14 0.09 0.09 1 0.11 0.08 0.06
Nup2-mAID 1 0.04 0.03 0.02 1 0.04 0.04 0.02
D
Fresh SDC+ Auxin
+ Auxin
Mid-log Culture (30°C)
30 min
20 min
ConA attachment
Imaging
E
+ Auxin
No degron
Nup2-mAID + Mlp1-mAID
Pom34-mCherry
2 µm
2 µm
F
Intrachromosomal Interactions
Chr. XII
HSP104 F+1550 / SSA2 F+1368
UBI4 F+524 / SSA2 F +1368
Normalized interaction frequency
HS
Min
G
Interchromosomal Interactions
Chr. XII / Chr.V
HSP104 F+1550 / SSA4 F+198
Chr. V / Chr. XII
SSA4 F+198 / SSA2 F+1368
HSP104 F+1550 / UBI4 F+524
Chr. XII / Chr. XVI
HSP104 F+1550 / HSP82 F+740
No degron
Nup2-mAID + Mlp1-mAID
H
Intragenic Interactions
SSA4 (Chr. V)
Enhancer-Promoter
F-268 / F+198
Promoter-Coding Region
F+198 / F+1079
Gene Looping
F+198 / F+2255

Figure 4. Double depletion of Nup2 and Mlp1 has no detectable effect on NPC integrity but significantly reduces heat shock-induced *HSR* intergenic and intragenic interactions.

(A) Relevant genotype of haploid strain SMY182, a haploid strain bearing *MLP1-mAID-MYC, NUP2-mAID-MYC* and *POM34-mCherry.*
(B) Experimental strategy for optimizing auxin concentration and incubation time.
(C) Immunoblot analysis of Mlp1-mAID-9Myc and Nup2-mAID-9Myc in cells treated with different concentrations of IAA for the indicated times. Detection and load control were as in Figure 2B.
(D) Experimental strategy for assessing NPC integrity upon simultaneous depletion of Mlp1 and Nup2. Cells expressing mCherry-tagged Pom34 bearing either no degron (SMY160) or the Mlp1-, Nup2- double degron (SMY182) were pretreated with 0.5 mM IAA at 30°C for 30 minutes, followed by attachment of cells on ConA-coated coverslips and imaging using widefield fluorescence microscopy (see Methods).
(E) Subnuclear localization of mCherry-tagged Pom34. Images were captured across 11 z planes with a step size of 0.5 microns. A representative plane of the Z stack is shown for each condition.
(F) & (G) Taq I-3C assay depicting *cis*- and *trans*-interactions between Hsf1-regulated genes in no degron (LRY016) and double degron (SMY152) strains. Cells were pretreated at 30°C with 0.5 mM of IAA for 30 min and then subjected to 3 min HS (39°C). All other steps and presentation of the data are as in Figure 3. Shown are means + SD, N=2, qPCR=4. To determine significance, an unpaired two-tailed t-test was performed. **, p<0.05; **, p<0.01, ***, p<0.001.*
(G) Intragenic interactions detected within the *SSA4* locus analyzed as above.

In thermally stressed cells, Nup2 and Mlp1 relocalize within the nucleus and are inducibly recruited to *HSR* genes

To gain insight into how Mlp1 and Nup2 impact 3D genome structure, we investigated the intranuclear location of each protein following exposure to acute HS. We tagged them with mNG and as shown in **Figure 5A**, both proteins, enriched at the nuclear periphery in the non-heat shock (NHS) state, rapidly relocalized in cells exposed to HS, and this was evident as early as 2.5 min. Nup2-mNG became diffusely distributed throughout the nucleoplasm, whereas Mlp1-mNG predominantly coalesced into several discrete puncta. Notably, a fraction of Mlp1 molecules remained diffusely distributed throughout the nucleoplasm throughout the heat shock time course.

Previous studies have suggested that Nup2 and Mlp1 physically associate with inducible genes upon their activation (Casolari et al., 2004; Schmid et al., 2006; Brickner et al., 2007; Luthra et al., 2007; Tan-Wong et al., 2009; Ahmed et al., 2010; Light et al., 2010; Brickner et al., 2012; Brickner et al., 2019) (see Table 1). Given their HS-induced intranuclear redistribution, we reasoned that Nup2 and Mlp1 may associate with Hsf1 target genes in a HS-dependent manner. To address this, we performed a chromatin immunoprecipitation (ChIP) assay over a similar heat shock time course. This analysis revealed enhanced association of both Nup2 and Mlp1 within regulatory and coding regions of *HSP104, HSP82* and *SSA4* in cells exposed to heat shock relative to

the control, non-induced state **(Figure 5B).** Consistent with its predominant presence within the nucleoplasm, Nup2 binding to these *HSR* genes was more rapid and of a greater magnitude than that of Mlp1. Notably, the association of each protein was transient, as occupancy in both cases peaked at 15 min and diminished thereafter. Importantly, the association of Nup2 and Mlp1 with a non-transcribed locus (*ARS504*) remained at near-background levels over the entire time course **(Figure 5B).**

Nup2 and Mlp1 are dispensable for the formation of heat shock-induced transcriptional condensates

Transcriptional condensates, enriched in Hsf1, Pol II and Mediator, form in response to heat shock and have been implicated in driving the spatial rearrangement of *HSR* genes (Chowdhary et al., 2022). It has been suggested that there is a functional linkage between Hsf1 condensate formation and *HSR* intergenic interactions (Chowdhary et al., 2019, 2022; Rubio et al., 2024). As described above, Nup2 and Mlp1 drive the coalescence of *HSR* genes **(Figures 4F** and **4G)** and this is likely mediated through heat shock-induced association of Nup2 and Mlp1 with such genes **(Figure 5B).** It was therefore of interest to investigate whether Nup2 and Mlp1 are required for the formation of heat shock-dependent Hsf1 condensates. To address this, we imaged Hsf1-mNG in no degron and double degron (Nup2-AID + Mlp1-AID) cells over a heat shock time course **(Figure 6A).** Hsf1 forms heat shock-dependent sub-nuclear clusters in parental, no degron cells **(Figures 6B, 6C),** confirming earlier observations (Chowdhary et al., 2019, 2022; Rubio et al., 2024). However, simultaneous depletion of Nup2 and Mlp1 had little or no effect. A similar outcome was evident in single deletion strains **(Figure 6D).** Consistent with these observations, neither Mlp1 nor Nup2 was enriched within Hsf1 condensates in heat shocked cells relative to the NHS control **(Figure S5).** Collectively, these results argue that Nup2 and Mlp1 promote *HSR* gene interactions without directly or indirectly participating in the formation of Hsf1 condensates.

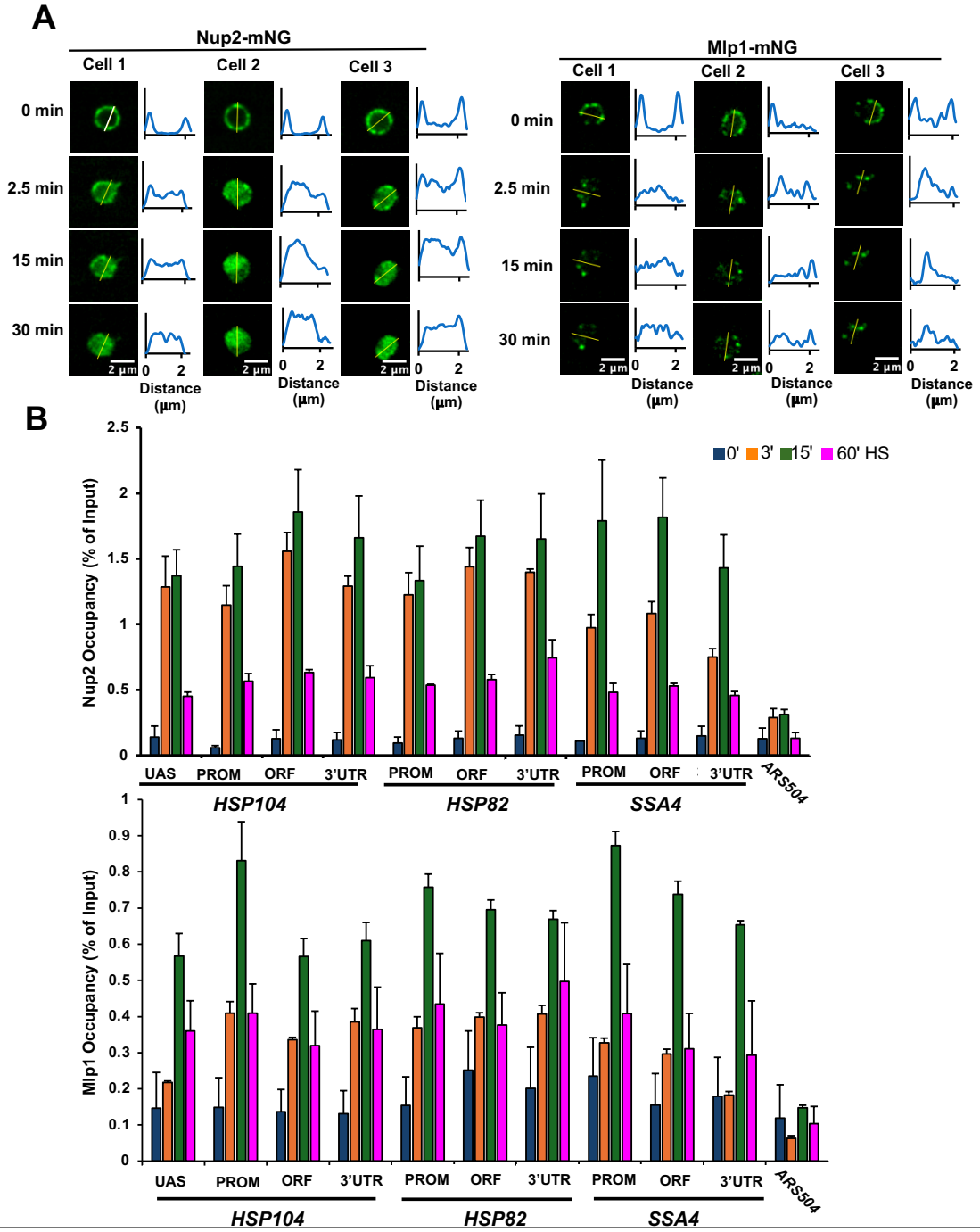

Figure 5. Nup2 and Mlp1 relocalize in cells exposed to heat shock and are rapidly recruited to *HSR* genes.

(A) *Left Panel Set:* Micrographs showing the distribution of Nup2-mNeonGreen (mNG) in SMY216 cells under NHS (25°C; 0 min) and HS (39°C) conditions. *Right Panel Set:* As above, except cells expressing Mlp1-mNG (SMY192) were evaluated. In both panels, a representative image of the Z stack is shown for each condition. Step size = 0.5 microns. The intensity plot profile on the right side of each image shows mNG signal distribution.

(B) Nup2 and Mlp1 occupancy of *HSR* genes is greatly enhanced following heat shock. Occupancy of the indicated loci – UAS, promoter (PROM), transcribed region (ORF) and 3'-UTR – was evaluated using ChIP-qPCR. Nup2-myc9- and Mlp1-myc9-tagged cells (SMY164 and SMY166, respectively) were subjected to the indicated duration of heat shock prior to HCHO-mediated crosslinking, chromatin isolation and immunoprecipitation with mAb 9E10 (see Methods). *ARS504* served as a non-transcribed negative control. Depicted are means + SD, N=2, qPCR=4.

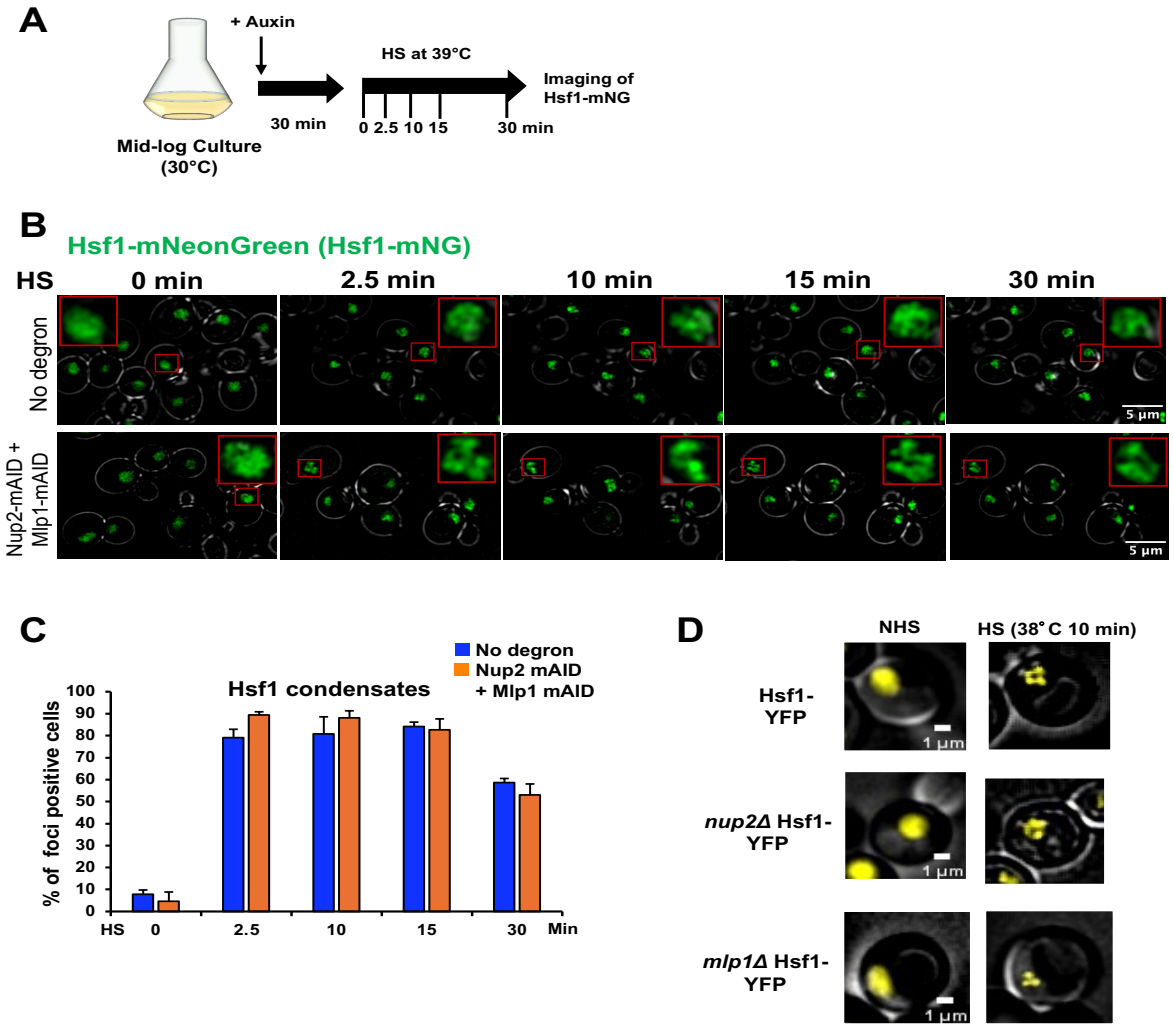

Figure 6. Formation of Hsf1 transcriptional condensates is unimpeded in Nup2-, Mlp1-depleted cells.

(A) Experimental strategy for live cell imaging. Mid-log phase cultures of Hsf1-mNG cells bearing no degron (SMY172) or the double Nup2-, Mlp1-degron (SMY170) were pretreated with 0.5 mM IAA for 30 min at 30°C, attached to a ConA-coated VAHEAT substrate, subjected to HS for the indicated times and then imaged on a confocal fluorescence microscope.

(B) Hsf1-mNG subnuclear localization in WT and Nup2-, Mlp1-depleted cells over the indicated HS time course. A representative image of the Z stack is shown for each condition. Step size: 0.56 microns. Insets are zoomed-in images of the indicated nuclei.

(C) Per cent SMY172 and SMY170 cells showing ≥2 Hsf1-mNG foci over a HS time course. An average of 150 cells per time point, per biological sample, were quantified using Imaris v.10.1.0. N=2. Values depicted are means + SD.

(D) Subnuclear localization of Hsf1-YFP in WT, *nup2Δ* and *mlp1Δ* cells (DPY032, SMY134 and SMY136, respectively) under NHS and HS conditions as indicated. Cells were imaged on a widefield fluorescence microscope. Depicted are representative Z-planes (step size 0.5 microns).

Nup2 and Mlp1 are not required for the recruitment of Hsf1 or Pol II to the *HSR* genes

Given that heat shock-induced Hsf1 clusters are associated with *HSR* genes (Chowdhary et al., 2022) and Hsf1 occupancy upstream of these genes increases significantly following a brief HS (Sekinger and Gross, 2001; Hahn et al., 2004; Kim and Gross, 2013; Pincus et al., 2018), we wished to know whether Nup2 and Mlp1 promote the occupancy of Hsf1 at representative UAS regions. To address this, we simultaneously depleted both proteins as above and performed ChIP following 0, 3 and 15 min of HS. This analysis indicated that Hsf1 occupancy was not affected by the simultaneous depletion of Nup2 and Mlp1 **(Figure 7A),** indicating that Nup2 and Mlp1 play little or no role in the recruitment of Hsf1.

We next asked whether Nup2 and Mlp2 are involved in recruiting Pol II to the *HSR* genes. We depleted Nup2 and Mlp1 together and performed ChIP as above. ChIP analysis demonstrated that simultaneous depletion of Nup2 and Mlp1 had no detectable effect on Pol II occupancy at either the promoter or coding region of representative *HSR* genes **(Figure 7B).** This finding indicates that Nup2 and Mlp1 are not critical for the heat shock-induced recruitment of Pol II to the *HSR* genes. Collectively, these observations suggest that double depletion of Nup2 and Mlp1 suppresses *HSR* gene coalescence in acute heat-shocked cells without diminishing the chromatin association of either Hsf1 or Pol II.

Nup2 and Mlp1 are not required for transcriptional induction of the *HSR* genes

It has been suggested that TF condensates are a key mechanism for transcriptional regulation (Hnisz et al., 2017; Cho et al., 2018; Sabari et al., 2018; Nair et al., 2019; Boija et al., 2021). Previous studies have noted that heat shock triggers strong transcriptional induction of *HSR* genes (Anandhakumar et al., 2016; Chowdhary et al., 2017; Pincus et al., 2018) and there is a temporal correlation between Hsf1 condensation and transcription in yeast cells exposed to acute heat shock (Chowdhary et al., 2019; Chowdhary et al., 2022; Rubio et al., 2024). In the experiments described above, we observed that simultaneous depletion of Nup2 and Mlp1 had no effect on

Hsf1 condensate formation. To ask whether simultaneous depletion of both proteins affects the heat shock-induced transcriptional activation of *HSR* genes, we conducted RT-qPCR **(Figure 8A).** We observed that double depletion of Nup2 and Mlp1 failed to impact *HSR* mRNA abundance under either the NHS or HS condition **(Figure 8B).** This finding is consistent with previous work which found that deletion of *MLP1* has no impact on the transcriptional activation of either *GAL10* or *HSP104* genes (Dieppois et al., 2006). It is also consistent with a recent study reporting that depletion of Nup2 does not affect genome-wide mRNA levels (Ge et al., 2024).

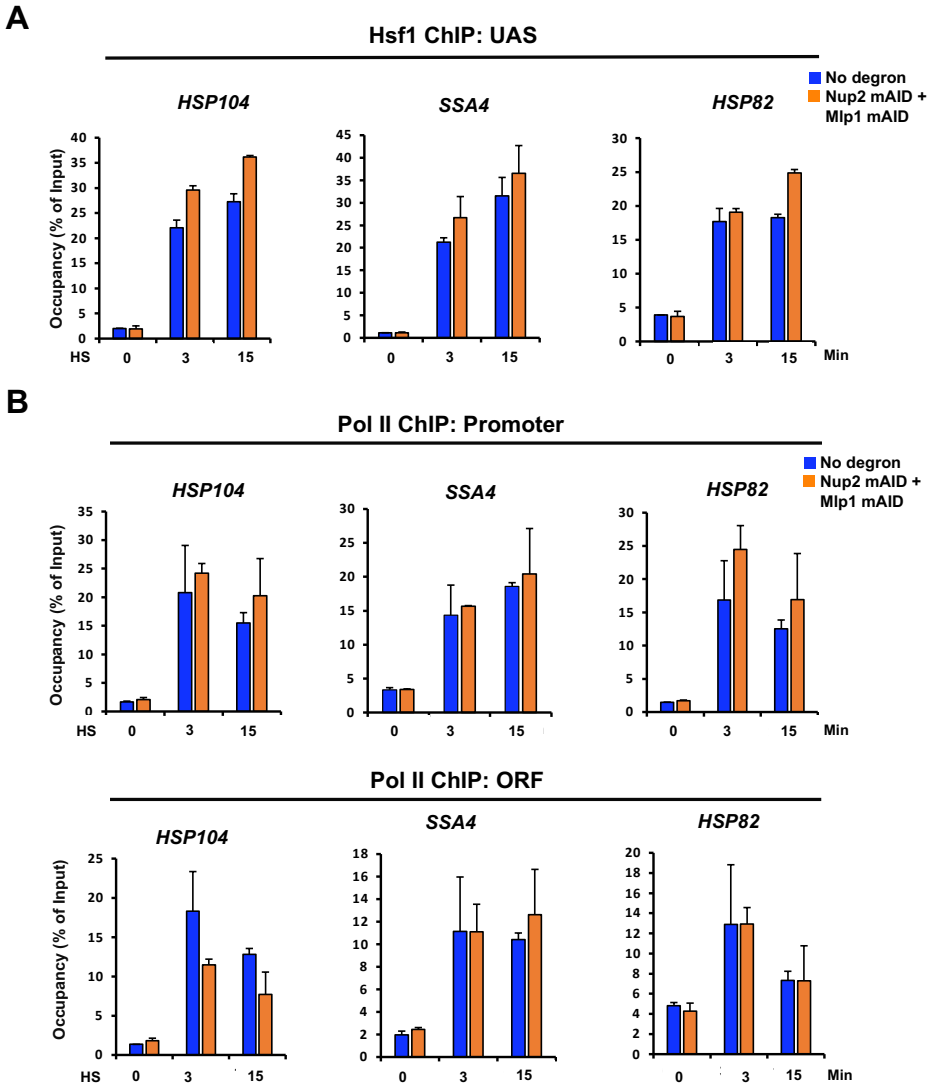

Figure 7. Hsf1 and Pol II occupancy of *HSR* genes is unimpeded in Nup2-, Mlp1-depleted cells.

(A) Hsf1 ChIP of the UAS regions of representative *HSR* genes in no degron (LRY016) and double degron (SMY152) strains pretreated with 0.5 mM IAA for 30 min before exposing them to HS for the indicated time points. Values are depicted as means + SD. N=2, qPCR=4

(B) Pol II ChIP of the promoter and ORF regions of representative *HSR* genes conducted in control and Nup2-, Mlp1-double depletion strains as in (A).

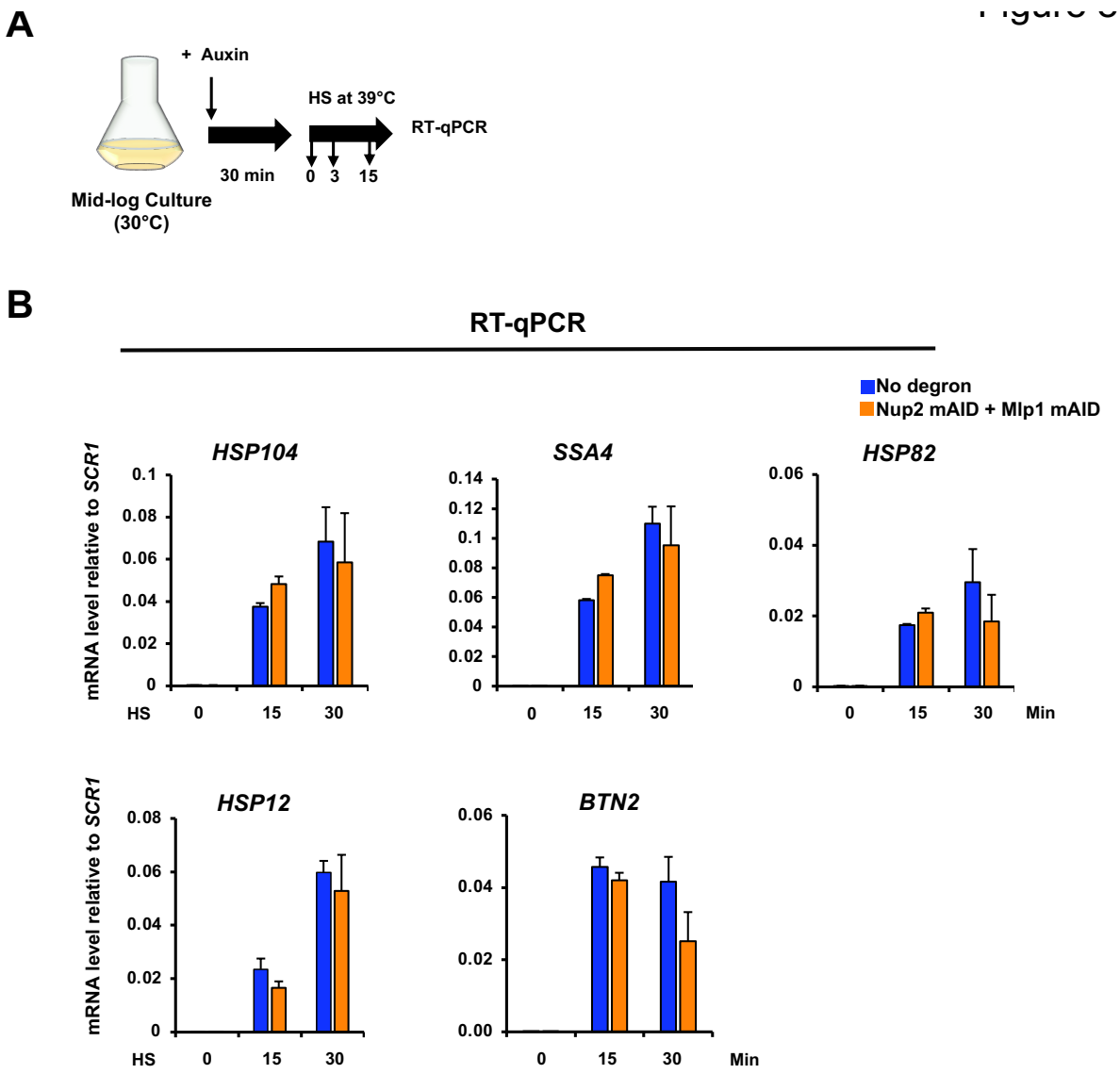

Figure 8. Transcriptional induction of *HSR* genes occurs unimpeded in Nup2-, Mlp1-depleted cells.

(A) Experimental strategy for assaying *HSR* transcript abundance. Mid-log phase (A_{600} =0.5) LRY016 (no degron) and SMY152 (Nup2- and Mlp1-double degron) cultures were grown in liquid YPDA and pretreated with 0.5 mM IAA for 30 min prior to exposing them to HS for the indicated durations. Total cell RNA was then isolated, and the indicated mRNAs were quantified by RT-qPCR.

(B) *HSR* mRNA levels in LRY016 and SMY152 cells were determined as described above and their abundance normalized to the Pol III transcript *SCR1*. Depicted are means + SD. N=2, qPCR=4.

Discussion

We have provided new insights into *HSR* gene coalescence (HGC) and the factors that contribute to the spatial repositioning of *HSR* genes. It has been previously observed that *HSR* genes can relocate to the NPC following their transcriptional activation (Dieppois et al., 2006; Brickner et al., 2019). Consistent with these earlier observations, we detect coalescence of *HSR* genes at the nuclear periphery. Far more frequently, however, such coalescence occurs within the nucleoplasm. Moreover, we have shown that the nuclear basket proteins Nup2 and Mlp1, inducibly recruited to *HSR* genes, are required to drive these genes into coalesced chromatin. We demonstrated this through simultaneous depletion of Nup2 and Mlp1 followed by 3C analysis in heat shock-induced cells. In contrast, using an analogous approach, we found that two essential NPC proteins, Nup1 and Nup145, play no detectable role. A previous study suggested that Nup1 is involved in subnuclear repositioning and interallelic clustering of *GAL1-10* genes (Brickner et al., 2016), yet we observed that depletion of Nup1 (in combination with Nup145) had minimal impact on *HSR* gene coalescence in HS-induced cells. Likewise, previous studies have suggested that inactivation of either Mlp1 or Nup2 obviated peripheral localization of transcriptionally induced *HSR* genes Dieppois et al., 2006; Brickner et al., 2019). However, we observed that ablation of either Mlp1 or Nup2 typically had only a mild effect on *HSR* gene clustering, as assessed by either microscopy or 3C. Therefore, this work has identified a specialized, albeit partially overlapping, role for Nup2 and Mlp1 in regulating yeast 3D genome organization.

Our findings contrast with the clustering of *MET* genes that occurs during methionine starvation (Li et al., 2024; Lee et al., 2024), as well as with the interallelic clustering of galactose-inducible and inositol starvation-inducible genes (Brickner et al., 2016) that occurs upon their transcriptional activation. In these cases, the clustering appears to occur at the NPC, and that NPC tethering promotes the transcription of these genes. In notable contrast, we show that *HSR* gene clustering occurs downstream of *HSR* transcriptional induction. Furthermore, as mentioned above, we show that *HSR* gene clustering occurs predominantly in the nucleoplasm and this fact,

in combination with the heat shock-induced subnuclear relocalization of Nup2 and Mlp1, argues that the nuclear basket proteins mediate their topological effects in an untethered, NPC-free state.

A second signature of the heat shock transcriptional response is the inducible formation of Hsf1 condensates that colocalize with *HSR* genes (Chowdhary et al., 2022), a phenomenon also observed in human cells (Zhang et al., 2022). In budding yeast, Hsf1 condensates form rapidly in response to acute HS (detectable within 2.5 min of a 30° to 39°C shift) but begin to return to a diffuse state as early as 30 min (this study and Chowdhary et al., 2019, 2022; Rubio et al., 2024). These condensates have been functionally linked to the 3D repositioning of *HSR* genes (Chowdhary et al., 2022). Several factors, including Hsf1, Pol II and Mediator, have been implicated in driving both Hsf1 condensate formation and HGC (Chowdhary et al., 2019, 2022; Rubio et al., 2024; Male et al., unpubl. observations). Nup2 and Mlp1 appear to represent a distinct category of nuclear factors, since they are required for *HSR* gene clustering yet unlike the aforementioned factors are dispensable for the formation of Hsf1 condensates. They also play no detectable role in the recruitment of either Hsf1 or Pol II to *HSR* genes. These results indicate that in response to HS, the formation of Hsf1 condensates and recruitment of Hsf1 and Pol II to the *HSR* genes can occur in the absence of long-range topological restructuring (see **Figure 9** for model).

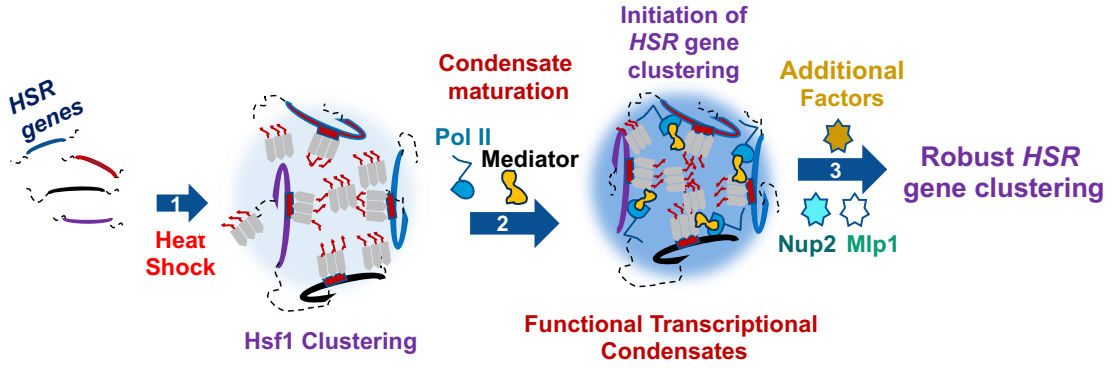

Figure 9. Model: Nup2 and Mlp1 promote *HSR* gene coalescence following their recruitment to these genes but without being incorporated into Hsf1 transcriptional condensates.

1. In response to heat shock, Hsf1 binds to the HSEs upstream of *HSR* genes (Hsf1 clustering). Some Hsf1 clusters may exist as clouds (Meeussen et al., 2023; Rubio et al., 2024).
2. RNA Pol II and Mediator are then recruited to the Hsf1 cluster and Hsf1 condensates undergo maturation (Chowdhary et al., 2022; Demmerle et al., 2023). This functional condensate is a precursor for initiating *HSR* gene transcription.
3. Following formation of Hsf1 condensates and transcriptional activation of Hsf1 target genes, Nup2 and Mlp1 are recruited to *HSR* genes but not detectably incorporated into Hsf1 condensates. This physical association with chromatin induces *HSR* gene clustering. (Data are also consistent with the nuclear basket proteins being recruited prior to, or simultaneous with, condensate formation and/or transcriptional activation.) The coalesced gene foci are predominantly detected within the nucleoplasm.

How might Nup2 and Mlp1 elicit their topological effect? Nup2 is involved in nucleocytoplasmic transport of proteins and RNA (Dilworth et al., 2001; Regot et al., 2013) while Mlp1 binds RNA export factors and participates in mRNA quality control and export (Green et al., 2003; Galy et al., 2004; Fasken et al., 2008;). Results presented here are consistent with these primary roles as we have shown that in heat shock-induced cells, Nup2 and Mlp1 [i] do not colocalize with heat shock-induced Hsf1 (as detected by live cell microscopy); [ii] do not impact either Hsf1 or RNA Pol II recruitment to *HSR* genes; and [iii] do not impact total *HSR* mRNA abundance. Yet both proteins undergo marked intranuclear relocalization upon HS and both physically associate with *HSR* genes. Given the predominant diffuse nucleoplasmic distribution of Nup2 and its strong occupancy of *HSR* genes, evident as early as 3 min following temperature upshift, Nup2 may directly drive *HSR* gene clustering via its ability to dynamically exchange between the nucleoplasm and NPC (Dilworth et al., 2001; Hakhverdyan et al., 2021). Although Mlp1 might contribute to this shuttle-and-clustering activity given its inducible occupancy of *HSR* genes, it is notable that most Mlp1 molecules condense into several discrete foci upon HS (this study and Carmody et al., 2010; Bensidoun et al., 2022). Therefore, Mlp1 condensates may promote HGC by sequestering one or more factors that inhibit *HSR* intergenic interactions. Of relevance to this postulated mechanism, heat shock-dependent sequestration of mRNA export factors was observed in Mlp1 foci in both budding and fission yeast (Carmody et al., 2010; Gallardo et al., 2020). This sequestration role may explain why we see a strong HGC phenotype despite the presence of Mlp2 (paralogue of Mlp1): either Mlp2 does not participate in the formation of such condensates or Mlp1/Mlp2 condensation may require a threshold concentration of the two proteins.

Consistent with our observations on the formation of enhancer - promoter, promoter - coding region, and promoter - 3'-UTR loops, Nup2 has previously been reported to exhibit boundary/insulator properties (Ishii et al., 2002; Dilworth et al., 2005) and Mlp1 has previously been implicated in gene looping (Tan-Wong et al., 2009). And as above, Nup2 might contribute directly via binding *HSR* genomic loci in the nuclear interior and foster their folding or looping as it transports them to the NPC. Mlp1 may

contribute to this activity, but it could enhance intragenic interactions via sequestration of one or more inhibitors of genome restructuring as argued above. Interestingly, none of these intergenic or intragenic perturbations materially impact the total abundance of *HSR* mRNA. These observations suggest that physical proximity between regulatory elements as detected by 3C analysis is unnecessary for robust Hsf1-driven transcription of its target genes. This is consistent with recent models of mammalian and *Drosophila* transcription that argue against the necessity of physical contact between enhancer and promoter elements to instigate transcriptional induction (Alexander et al., 2019; Heist et al., 2019; Espinola et al., 2021).

Conclusions

In conclusion, our observations reveal a novel, highly specific role for the nuclear basket proteins Nup2 and Mlp1 in promoting the 3D repositioning and coalescence of heat shock-induced *HSR* genes. This role is likely served when these proteins are in their NPC-free, diffusive state. Other phenomena associated with the heat shock transcriptional response – Hsf1 condensate formation, Hsf1 binding to upstream regulatory regions of *HSR* genes, Pol II recruitment, and transcription of *HSR* genes – occur independently of Nup2 and Mlp1. In this regard, our work has identified a unique category of factors, since other factors thus far characterized in the *HSR* lack such specificity and appear to participate in most if not all steps (Chowdhary et al., 2019, 2022; Rubio et al., 2024).

The findings presented here provide further evidence that Hsf1 condensate formation can be uncoupled from downstream events in the HSR. We recently showed that in response to 8.5% ethanol stress, Hsf1 condensates form, and *HSR* genes reposition, well before *HSR* genes are transcriptionally activated (Rubio et al., 2024). Here, we have demonstrated that in response to thermal stress, Hsf1 condensate formation can occur without downstream *HSR* gene repositioning in Nup2-, Mlp1-depleted cells. Further research into molecular mechanisms of how Nup2 and Mlp1 are recruited to *HSR* genes and reshape *HSR* gene topology and the biological relevance of Hsf1 condensate formation and *HSR* gene coalescence will enhance our understanding of how cells respond to thermal stress and maintain cellular homeostasis.

Materials and Methods

Yeast Strain Construction

For microscopy analyses, to construct SMY206, we initially PCR-amplified the *KAN-MX* gene from pFA6a-KanMX6 using forward and reverse chimeric primers containing ~50 bp of *HSP82* after the poly (A) site juxtaposed against 20 bp sequence homologous to the plasmid. We transformed ASK726 with the PCR amplicon to insert *KAN-MX* downstream of the *HSP82* gene, creating SMY108. *KAN-MX* served as a landing pad to insert $TetO_{200}$*::LEU2*. (Note: actual TetO repeat length is likely <200 bp.) The plasmid pSR14 ($TetO_{200}$*::LEU2),* kindly provided by S. Gasser, Friedrich Miescher Institute for Biomedical Research, was linearized with Asc I, creating homologous ends for *KAN-MX*. The linearized $TetO_{200}$*::LEU2* was inserted into the *KAN-MX* locus, creating SMY109. SMY118 was created by crossing SMY109 with W303-1B, followed by sporulation, tetrad dissection, and selection of a haploid bearing only the *LEU2* marker. SMY110 was created by crossing ASK701 with W303-1A followed by sporulation, tetrad dissection, and selection of a haploid with only the *TRP1* marker. Plasmid pMY63 (*REV1pr-tetR-mCherry*, *REV1pr-lacI-GFP*), a gift of Lu Bai, Penn State University, was then linearized by digestion with BsiWI and inserted into the *his3* locus of SMY110, creating SMY123. The SMY206 diploid was generated by crossing SMY123 and SMY118.

Strain SMY207 was constructed by crossing SMY123 and SMY118 following deletion of *MLP1* from both strains using the *mlp1Δ::KAN-MX* PCR product as transforming DNA (genomic template obtained from the ResGen KO strain). SMY208 was generated in a similar fashion using *nup2Δ::KAN-MX* as the transforming DNA. SMY201 was constructed by crossing ASK722 x ASK726 following deletion of *NUP2* from both strains using *nup2Δ::KAN-MX*. SMY203 was generated in a similar fashion using *mlp1Δ::KAN-MX*. SMY134 and SMY136 were generated by deleting *NUP2* and *MLP1*, respectively, from DPY032. SMY160, SMY163, and SMY182 were created by transforming LRY016, SMY148, and SMY152, respectively, with *POM34-mCherry::NAT* using JTY001 genomic DNA as a template. SMY170 and SMY172 were constructed by transforming SMY152 and LRY016, respectively, with *HSF1-mNeonGreen::HIS5* using LRY037

genomic DNA as a template. SMY192 and SMY196 were constructed by in-frame insertion of *mNeonGreen::HIS5* at the C- terminus of *MLP1* in LRY016 and SMY148, respectively. SMY216 and SMY221 were constructed in a similar fashion by targeting the C- terminus of *NUP2* in LRY016 and SMY148. The plasmid template for these amplifications was pFA6a-link-ymNeonGreen-SpHis5. Finally, LRY777 and LRY888 were constructed by transforming SMY192 and SMY216, respectively, with the *HSF1*-targeted *mCherry::URA3* amplicon.

For molecular analyses, SMY143 and SMY145 were constructed by introducing a mini-degron tag amplified from *pKAN-mAID*-9myc* (Morawska and Ulrich, 2013) into LRY016, respectively, targeting the C-termini of *NUP1* and *MLP1*. Similarly, strains SMY148, SMY149, and SMY152 were generated by introducing a mini-degron tag PCR amplified from *pHyg-mAID*-9myc* (Morawska and Ulrich, 2013) into the C-terminus of *NUP145* in SMY143, *NUP2* in LRY016, and *NUP2* in SMY145, respectively. SMY164 and SMY166 were constructed by in-frame insertion of a *Myc9::TRP1* tag at the C terminus of *NUP2* and *MLP1* in strain LRY016 using pWZV87 as PCR template.

See Tables S1, S2, and S3 for complete lists of strains, plasmids, and primers used in strain construction.

Yeast Culture and Treatment Conditions

Yeast cells were grown overnight (O/N) in liquid YPDA (1% w/v yeast extract, 2% w/v peptone, 2% w/v dextrose, and 20 mg/L adenine). Cells from the overnight cultures were inoculated into fresh liquid YPDA and allowed to grow at 30°C until they reached mid-log density (OD_{600} = 0.5 to 0.8). To induce heat shock, the mid-log phase culture was combined with an equal volume of YPDA medium preheated to 55°C to elicit an instantaneous 25°C to 39°C shift. The culture was then maintained at 39°C for the specified duration. Control samples without heat stress were diluted with an equal volume of YPDA and kept at 25°C. All samples were maintained at their respective temperatures using a water bath with continuous shaking.

Auxin-Induced Degradation (AID) and Immunoblot Analysis

The proteins of interest used in this study were degraded using the AID strategy (Morawska and Ulrich, 2013). To optimize auxin concentration and incubation time, actively growing (OD_{600}=0.5) degron-tagged cells expressing the F-box protein osTIR1 were treated with different concentrations of indoleacetic acid (0.5 or 1 mM IAA) at 30°C for 0, 20, 30 and 60 min before undergoing metabolic arrest with 20 mM sodium azide, followed by cell harvesting. Fresh IAA stocks (100 mg/mL [570 mM]) were prepared in 95% ethanol and sterilized by filtration before use. For the control (0 min) sample, cells were treated with an equal volume of vehicle alone.

The harvested cells were subjected to protein extraction and immunoblot analysis as previously described (Rubio and Gross, 2023). Monoclonal antibodies (mAbs) targeting Myc (9E10; Santa Cruz Biotechnology sc-40) and Pgk1 (ThermoFisher 459250) were used in the immunoblot analysis.

For 3C, ChIP, and RT-qPCR analysis, mid-log cells grown in YPDA were treated with 1 mM IAA for 60 min (for LRY016 and SMY148) or 0.5 mM IAA with 30 mins (for LRY016, SMY145, SMY149 and SMY152) prior to +/- heat shock for the specified time points. Auxin concentrations were kept constant throughout the experiment (+/- HS) to ensure continuous degradation of the target proteins.

Spot Dilution Assay

O/N cultures grown in YPDA at 30°C were diluted to OD_{600}=0.5 using sterile distilled water. Cells were then serially diluted 1:5 and 7 μl of each dilution were spotted on YPDA plates using a 20 μl pipette. The plates were incubated for 36 to 48 hours at 24°C, 30°C, 35°C, and 37°C **(Figure S3).**

Cell Viability Assay

Mid-log cells (OD_{600}=0.5), obtained following inoculation of fresh liquid YPDA medium with an O/N culture, were exposed to heat shock (39°C) for the indicated time points (Fig. S3) using the method described above. Cultures were diluted 1: 10,000 and

plated onto YPDA plates. Plates were incubated at 30°C for 36 to 48 hours. Colonies were counted and the average number from two replicates was plotted on a bar graph. For the Nup2 and Mlp1-double degron-tagged strain (SMY152), mid-log cells (OD_{600} 0.5), obtained following inoculation of fresh liquid YPDA medium with an O/N culture, were treated with 0.5 mM auxin (IAA) or vehicle alone for 30 min at 30°C. These cells were then subjected to +/-heat shock, as mentioned above. Auxin concentration was maintained throughout and cells from each heat shock time point were collected, diluted, and plated onto YPDA plates.

Taq I Chromosome Conformation Capture (Taq I-3C)

Taq I-3C (Chowdhary et al., 2020) was performed essentially as described (Rubio and Gross, 2023). From O/N cultures, a master cell culture was inoculated and grown in liquid YPDA at 30°C, starting from an initial OD_{600} of 0.15 and reaching a final OD_{600} of 0.65 to 0.7 before subjecting the cultures to +/- HS. For each experimental condition (NHS and HS), 50 mL aliquots of cultures were used. Heat shock was performed as described above. Target proteins were degraded using the AID strategy outlined above before exposing the cells to heat shock. Primers used for analyzing the 3C templates are listed in Supplemental File 1 - Table S6.

Reverse Transcription - Quantitative PCR (RT-qPCR)

RT-qPCR was performed as previously described (Rubio and Gross, 2023). PCR primers used for this analysis are listed in Supplemental File 1—Table S4. Target proteins were conditionally degraded as described above before exposing the cells to heat shock**.**

Chromatin Immunoprecipitation (ChIP)

Hsf1 and Pol II ChIP assays were performed as previously described (Rubio et al., 2024) using rabbit antisera raised in our laboratory (Venturi et al., 2000; Zhao et al., 2005). For Nup2 and Mlp1 ChIP, sonicated chromatin lysates were incubated with 2.5 µL of anti-Myc antibody, and the antibody-bound chromatin fragments were captured on

Protein G-Sepharose beads (GE Healthcare) by incubating for 16 h at 4°C. All other steps were conducted as previously described (Rubio et al., 2024). Primers used in the ChIP analysis are listed in Supplemental File 1 – Table S5.

Fluorescence Microscopy

Widefield Microscopy

Live cell imaging of NHS and HS states **(Figures 1C, 2F, 4E, 6D** and **S2)** was performed essentially as described (Rubio et al., 2024) using an AX70 Olympus epifluorescence microscope equipped with an Olympus Ach 100/1.25-NA objective. Briefly, mid-log phase (A_{600} =0.6) cells grown in synthetic dextrose complete (SDC) medium, inoculated from an O/N culture, were incubated on a concanavalin A (Con A)-coated coverslip for 20 min and then subjected to instantaneous heat shock (25°C to 38°C) for the indicated time points. For **Figures 2F** and **4E,** cells were pretreated with the specified concentration of auxin (see AID strategy) prior to attachment on the Con A-coated coverslip, followed by imaging at 25°C. Images were captured across nine z planes (**Figure S2B)**, 11 z planes **(Figures 1C, 2F, 4E)** or 4 to 6 z planes **(Figure 6D)** with a step size of 0.5 microns. Typically, ~100 cells were counted per biological sample per time point. Note that in **Figure 6D**, Hsf1-mYFP foci were processed using the smooth and sharpen image processing functions in FIJI/ImageJ.

Spinning Disk Confocal Microscopy

Live cell imaging of mid-log cultures in **Figures 2D, 2E, 5A, 6B, 6C** and **S5** was performed on an Olympus CSU W1 Spinning Disk Confocal System equipped with an UPlan Apo 100x/1.50 NA objective coupled to a sCMOS camera controlled by cellSens Dimension software as described (Rubio et al., 2024). In **Figures 2D** and **2E,** mid-log cells were pretreated with vehicle alone or auxin prior to attachment on a Con A-coated VAHEAT (Interherence Gmbh) substrate, followed by imaging at 25°C. In all other figures, mid-log cells were treated similarly (where appropriate) before attaching them to a ConA-coated VAHEAT substrate, followed by instantaneous heat shock (25°C to 39°C) for the indicated time points. Images were captured across 21 z planes with a step size of 0.3 µm for **Figure 2D**, 10 z planes with a step size of 0.56 µm for **Figure**

6B, and 11 z planes with a step size of 0.5 μm for **Figures 5A** and **S5**. ∽100 cells were counted per biological sample per time point.

Image reconstruction and analysis were done using FIJI/ImageJ (v. 1.53t) (Schindelin et al., 2012). NPC integrity was determined by examining subcellular localization of the Pom34-mCherry signal and the percentage of cells exhibiting Pom34-mCherry punctate structure **(Figure 2E)** was counted manually. Quantification of cells with Hsf1-mNeonGreen foci **(Figure 6C)** was performed using the "Cells" feature in Imaris v.10.1.0. Cells with 2 or more foci were included in the Hsf1-mNG foci analysis. The diameters of the nucleus and Hsf1 foci were set to 2 μm and 0.48 μm, respectively, in Imaris. For the analysis of Hsf1 foci-containing cells, the nuclear volume ranged from 0.8 to 4 μm^3. For **Figures 6B** and **6C**, image deconvolution was performed using the Weiner plugin in CellSens Dimension software. In **Figure S2B**, the quantification of cells with *HSR* gene coalescence was accomplished by manually counting the number of cells displaying overlapping green and red dots.

Statistical Tests

The statistical significance of the differences in mean values for various assays was determined using Microsoft Excel, as specified in the figure legends. A two-tailed, unpaired “t” test with equal variance was performed in each case.

Online Supplemental Material

Fig. S1 presents the locations of primers used in 3C analysis and physical maps of Hsf1-regulated genes evaluated in this study. Fig. S2 shows the impact of deletion or conditional depletion of either Nup2 or Mlp1 on *HSR* gene interactions in acutely heat-shocked cells. Fig. S3 presents viability and growth fitness assays of cells depleted of either Nup2 or Mlp1 (or both). Fig. S4 demonstrates the impact of double depletion of Nup2 and Mlp1 on the frequency of intragenic looping within *HSP104* in acutely heat-shocked cells. Fig. S5 shows the subcellular distribution of Mlp1, Nup2 and Hsf1 under control and acute heat shock conditions. Tables S1 and S2 list the yeast strains and

plasmids used in this study. Tables S3, S4, S5 and S6 provide sequences of primers used in strain construction, RT-qPCR, ChIP, and TaqI-3C.

Acknowledgments

We thank Drs. David Pincus, Kelly Tatchell, Arrigo De Benedetti, Jason M. Bodily, Surabhi Chowdhary and Gurranna Male for insightful discussions and technical advice. We thank Dr. Amoldeep Kainth for strain construction and Paula Polk and Dr. Malgorzata Bienkowska-Haba for assistance in the Research Core Facility. We are grateful to Drs. Chabbi Govind (Oakland University); Helle D. Ulrich (Institute of Molecular Biology gGmbH); Susan Gasser (Friedrich Miescher Institute for Biomedical Research); Jurg Bahler (University College London); John Pringle (Stanford University School of Medicine); Bas Teusink (Vrije Universiteit Amsterdam); Kim Nasmyth (Research Institute of Molecular Pathology; and Lu Bai (Penn State University) for providing plasmids and reagents. We also appreciate the generosity of Drs. David Pincus, Kelly Tatchell, Amoldeep Kainth, and Donna and Jason Brickner for providing yeast strains. This work was supported by NIH grants R15 GM128065 and R01 GM138988 awarded to D.S.G. and Ike Muslow predoctoral fellowships awarded to S.M. and L.S.R.

References

Ahmed, S., D.G. Brickner, W.H. Light, I. Cajigas, M. McDonough, A.B. Froyshteter, T. Volpe, and J.H. Brickner. 2010. DNA zip codes control an ancient mechanism for gene targeting to the nuclear periphery. *Nat Cell Biol*. 12:111–118. doi:10.1038/ncb.2011.

Ahn, J.H., E.S. Davis, T.A. Daugird, S. Zhao, I.Y. Quiroga, H. Uryu, J. Li, A.J. Storey, Y.H. Tsai, D.P. Keeley, S.G. Mackintosh, R.D. Edmondson, S.D. Byrum, L. Cai, A.J. Tackett, D. Zheng, W.R. Legant, D.H. Phanstiel, and G.G. Wang. 2021. Phase separation drives aberrant chromatin looping and cancer development. *Nature*. 595:591–595. doi:10.1038/s41586-021-03662-5.

Aitchison, J.D., and M.P. Rout. 2012. The yeast nuclear pore complex and transport through it. *Genetics*. 190:855–883. doi:10.1534/genetics.111.127803.

Akey, C.W., D. Singh, C. Ouch, I. Echeverria, I. Nudelman, J.M. Varberg, Z. Yu, F. Fang, Y. Shi, J. Wang, D. Salzberg, K. Song, C. Xu, J.C. Gumbart, S. Suslov, J. Unruh, S.L. Jaspersen, B.T. Chait, A. Sali, J. Fernandez-Martinez, S.J. Ludtke, E. Villa, and M.P. Rout. 2022. Comprehensive structure and functional adaptations of the yeast nuclear pore complex. *Cell*. 185:361–378. doi:10.1016/j.cell.2021.12.015.

Alber, F., S. Dokudovskaya, L.M. Veenhoff, W. Zhang, J. Kipper, D. Devos, A. Suprapto, O. Karni-Schmidt, R. Williams, B.T. Chait, A. Sali, and M.P. Rout. 2007. The molecular architecture of the nuclear pore complex. *Nature*. 450:695–701. doi:10.1038/nature.06405.

Alexander, J.M., J. Guan, B. Li, L. Maliskova, M. Song, Y. Shen, B. Huang, S. Lomvardas, and O.D. Weiner. 2019. Live-cell imaging reveals enhancer-dependent sox2 transcription in the absence of enhancer proximity. *Elife*. 8:e41769. doi:10.7554/elife.41769.

Anandhakumar, J., Y.W. Moustafa, S. Chowdhary, A.S. Kainth, and D.S. Gross. 2016. Evidence for multiple Mediator complexes in yeast independently recruited by activated heat shock factor. *Mol Cell Biol*. 36:1943-1960. doi:10.1128/mcb.00005-16.

Ansari, A., and M. Hampsey. 2005. A role for the CPF 3′-end processing machinery in RNAP II-dependent gene looping. *Genes Dev*. 19:2969–2978. doi:10.1101/gad.1362305.

Babokhov, M., K. Hibino, Y. Itoh, and K. Maeshima. 2020. Local chromatin motion and transcription. *J Mol Biol*. 432:694–700. doi:10.1016/j.jmb.2019.10.018.

Bähler, J., J.Q. Wu, M.S. Longtine, N.G. Shah, A. McKenzie 3rd, A.B. Steever, A. Wach, P. Philippsen, and J.R. Pringle. 1998. Heterologous modules for efficient and versatile PCR-based gene targeting in Schizosaccharomyces pombe. *Yeast*. 14:943–951. doi:10.1002/(sici)1097-0061(199807)14:10<943::aid-yea292>3.0.co;2-y.

Beck, M., F. Förster, M. Ecke, J.M. Plitzko, F. Melchior, G. Gerisch, W. Baumeister, and O. Medalia. 2004. Nuclear pore complex structure and dynamics revealed by cryoelectron tomography. *Science*. 306:1387–1390. doi:10.1126/science.1104808.

Bensidoun, P., T. Reiter, B. Montpetit, D. Zenklusen, and M. Oeffinger. 2022. Nuclear mRNA metabolism drives selective basket assembly on a subset of nuclear pore complexes in budding yeast. *Mol Cell*. 82:3856–3871. doi:10.1016/j.molcel.2022.09.019.

Boija, A., I.A. Klein, and R.A. Young. 2021. Biomolecular condensates and cancer. *Cancer Cell*. 39:174–192. doi:10.1016/j.ccell.2020.12.003.

Bolte, S., and F.P. Cordelières. 2006. A guided tour into subcellular colocalization analysis in light microscopy. *J Microsc*. 224:213–232. doi:10.1111/J.1365-2818.2006.01706.X.

Botman, D., D.H. de Groot, P. Schmidt, J. Goedhart, and B. Teusink. 2019. In vivo characterisation of fluorescent proteins in budding yeast. *Sci Rep*. 9:2234. doi:10.1038/s41598-019-38913-z.

Brickner, D.G., S. Ahmed, L. Meldi, A. Thompson, W. Light, M. Young, T.L. Hickman, F. Chu, E. Fabre, and J.H. Brickner. 2012. Transcription factor binding to a DNA zip code controls interchromosomal clustering at the nuclear periphery. *Dev Cell*. 22:1234–1246. doi:10.1016/j.devcel.2012.03.012.

Brickner, D.G., and J.H. Brickner. 2010. Cdk phosphorylation of a nucleoporin controls localization of active genes through the cell cycle. *Mol Biol Cell*. 21:3421–3432. doi:10.1091/mbc.E10-01-0065.

Brickner, D.G., and J.H. Brickner. 2012. Interchromosomal clustering of active genes at the nuclear pore complex. *Nucleus*. 3:487–492. doi:10.4161/nucl.22663.

Brickner, D.G., I. Cajigas, Y. Fondufe-Mittendorf, S. Ahmed, P.C. Lee, J. Widom, and J.H. Brickner. 2007. H2A.Z-mediated localization of genes at the nuclear periphery confers epigenetic memory of previous transcriptional state. *PLoS Biol*. 5:e81. doi:10.1371/j.pbio.0050081.

Brickner, D.G., R. Coukos, and J.H. Brickner. 2015. INO1 transcriptional memory leads to DNA zip code-dependent interchromosomal clustering. *Microbial Cell*. 2:481–490. doi:10.15698/mic.2015.12.242.

Brickner, D.G., C. Randise-Hinchliff, M.L. Corbin, J.M. Liang, S. Kim, B. Sump, A. D'Urso, S.H. Kim, A. Satomura, H. Schmit, R. Coukos, S. Hwang, R. Watson, and J.H. Brickner. 2019. The role of transcription factors and nuclear pore proteins in controlling the spatial organization of the yeast genome. *Dev Cell*. 49:936-947.e4. doi:10.1016/j.devcel.2019.05.023.

Brickner, D.G., V. Sood, E. Tutucci, R. Coukos, K. Viets, R.H. Singer, and J.H. Brickner. 2016. Subnuclear positioning and interchromosomal clustering of the GAL1-10 locus are controlled by separable, interdependent mechanisms. *Mol Biol Cell*. 27:2980–2993. doi:10.1091/mbc.E16-03-0174.

Brickner, J.H., and P. Walter. 2004. Gene recruitment of the activated INO1 locus to the nuclear membrane. *PLoS Biol*. 2:e342. doi:10.1371/j.pbio.0020342.

Cabal, G.G., A. Genovesio, S. Rodriguez-Navarro, C. Zimmer, O. Gadal, A. Lesne, H. Buc, F. Feuerbach-Fournier, J.C. Olivo-Marin, E.C. Hurt, and U. Nehrbass. 2006. SAGA interacting factors confine sub-diffusion of transcribed genes to the nuclear envelope. *Nature*. 441:770–773. doi:10.1038/nature.04752.

Carmody, S.R., E.J. Tran, L.H. Apponi, A.H. Corbett, and S.R. Wente. 2010. The mitogen-activated protein kinase Slt2 regulates nuclear retention of non-heat shock mRNAs during heat shock-induced stress. *Mol Cell Biol*. 30:5168–5179. doi:10.1128/mcb.00735-10.

Casolari, J.M., C.R. Brown, D.A. Drubin, O.J. Rando, and P.A. Silver. 2005. Developmentally induced changes in transcriptional program alter spatial

organization across chromosomes. *Genes Dev*. 19:1188–1198. doi:10.1101/gad.1307205.

Casolari, J.M., C.R. Brown, S. Komili, J. West, H. Hieronymus, and P.A. Silver. 2004. Genome-wide localization of the nuclear transport machinery couples transcriptional status and nuclear organization. *Cell*. 117:427–439. doi:10.1016/S0092-8674(04)00448-9.

Cho, W.K., J.H. Spille, M. Hecht, C. Lee, C. Li, V. Grube, and I.I. Cisse. 2018. Mediator and RNA polymerase II clusters associate in transcription-dependent condensates. *Science*. 361:412–415. doi:10.1126/science.aar4199.

Chowdhary, S., A.S. Kainth, and D.S. Gross. 2017. Heat shock protein genes undergo dynamic alteration in their three-dimensional structure and genome organization in response to thermal stress. *Mol Cell Biol*. 37:e00292-17. doi:10.1128/mcb.00292-17.

Chowdhary, S., A.S. Kainth, and D.S. Gross. 2020. Chromosome conformation capture that detects novel cis- and trans-interactions in budding yeast. *Methods*. 170:4–16. doi:10.1016/j.ymeth.2019.06.023.

Chowdhary, S., A.S. Kainth, S. Paracha, D.S. Gross, and D. Pincus. 2022. Inducible transcriptional condensates drive 3D genome reorganization in the heat shock response. *Mol Cell*. 82:4386-4399.e7. doi:10.1016/j.molcel.2022.10.013.

Chowdhary, S., A.S. Kainth, D. Pincus, and D.S. Gross. 2019. Heat shock factor 1 drives intergenic association of its target gene loci upon heat shock. *Cell Rep*. 26:18-28.e5. doi:10.1016/j.celrep.2018.12.034.

Cosma, M.P., T. Tanaka, and K. Nasmyth. 1999. Ordered recruitment of transcription and chromatin remodeling factors to a cell cycle– and developmentally regulated promoter. *Cell*. 97:299–311. doi:10.1016/s0092-8674(00)80740-0.

Dekker, J., and L. Mirny. 2016. The 3D genome as moderator of chromosomal communication. *Cell*. 164:1110–1121. doi:10.1016/j.cell.2016.02.007.

Dekker, M., E. Van Der Giessen, and P.R. Onck. 2023. Phase separation of intrinsically disordered FG-Nups is driven by highly dynamic FG motifs. *Proc Natl Acad Sci U S A*. 120:e2221804120. doi:10.1073/pnas.2221804120.

Demmerle, J., S. Hao, and D. Cai. 2023. Transcriptional condensates and phase separation: condensing information across scales and mechanisms. *Nucleus*. 14:2213551. doi:10.1080/19491034.2023.2213551.

Denning, D.P., S.S. Patel, V. Uversky, A.L. Fink, and M. Rexach. 2003. Disorder in the nuclear pore complex: the FG repeat regions of nucleoporins are natively unfolded. *Proc Natl Acad Sci U S A*. 100:2450–2455. doi:10.1073/pnas.0437902100.

Denoth-Lippuner, A., M.K. Krzyzanowski, C. Stober, and Y. Barral. 2014. Role of SAGA in the asymmetric segregation of DNA circles during yeast ageing. *Elife*. 3:e03790. doi:10.7554/elife.03790.

Dieppois, G., N. Iglesias, and F. Stutz. 2006. Cotranscriptional recruitment to the mRNA export receptor Mex67p contributes to nuclear pore anchoring of activated genes. *Mol Cell Biol*. 26:7858–7870. doi:10.1128/mcb.00870-06.

Dieppois, G., and F. Stutz. 2010. Connecting the transcription site to the nuclear pore: a multi-tether process that regulates gene expression. *J Cell Sci*. 123:1989–1999. doi:10.1242/jcs.053694.

Dilworth, D.J., A. Suprapto, J.C. Padovan, B.T. Chait, R.W. Wozniak, M.P. Rout, and J.D. Aitchison. 2001. Nup2p dynamically associates with the distal regions of the Yeast nuclear pore complex. *J Cell Biol*. 153:1465–1478. doi:10.1083/jcb.153.7.1465.

Dilworth, D.J., A.J. Tackett, R.S. Rogers, E.C. Yi, R.H. Christmas, J.J. Smith, A.F. Siegel, B.T. Chait, R.W. Wozniak, and J.D. Aitchison. 2005. The mobile nucleoporin Nup2p and chromatin-bound Prp20p function in endogenous NPC-mediated transcriptional control. *J Cell Biol*. 171:955–965. doi:10.1083/jcb.200509061.

Dockendorff, T.C., C. V. Heath, A.L. Goldstein, C.A. Snay, and C.N. Cole. 1997. C-terminal truncations of the yeast nucleoporin Nup145p produce a rapid temperature-conditional mRNA export defect and alterations to nuclear structure. *Mol Cell Biol*. 17:906–920. doi:10.1128/mcb.17.2.906.

Du, M., F. Zou, Y. Li, Y. Yan, and L. Bai. 2022. Chemically Induced Chromosomal Interaction (CICI) method to study chromosome dynamics and its biological roles. *Nat Commun*. 13:757. doi:10.1038/s41467-022-28416-3.

Dultz, E., H. Tjong, E. Weider, M. Herzog, B. Young, C. Brune, D. Müllner, C. Loewen, F. Alber, and K. Weis. 2016. Global reorganization of budding yeast chromosome conformation in different physiological conditions. *J Cell Biol*. 212:321–334. doi:10.1083/jcb.201507069.

Espinola, S.M., M. Götz, M. Bellec, O. Messina, J.B. Fiche, C. Houbron, M. Dejean, I. Reim, A.M. Cardozo Gizzi, M. Lagha, and M. Nollmann. 2021. Cis-regulatory chromatin loops arise before TADs and gene activation, and are independent of cell fate during early Drosophila development. *Nat Genet*. 53:477–486. doi:10.1038/s41588-021-00816-z.

Fabre, E., W.C. Boelens, C. Wimmer, I.W. Mattaj, and E.C. Hurt. 1994. Nup145p is required for nuclear export of mRNA and binds homopolymeric RNA in vitro via a novel conserved motif. *Cell*. 78:275–289. doi:10.1016/0092-8674(94)90297-6.

Fasken, M.B., M. Stewart, and A.H. Corbett. 2008. Functional significance of the interaction between the mRNA-binding protein, Nab2, and the nuclear pore-associated protein, Mlp1, in mRNA Export. *J Biol Chem*. 283:27130-27143. doi:10.1074/jbc.M803649200.

Fernandez-Martinez, J., J. Phillips, M.D. Sekedat, R. Diaz-Avalos, J. Velazquez-Muriel, J.D. Franke, R. Williams, D.L. Stokes, B.T. Chait, A. Sali, and M.P. Rout. 2012. Structure–function mapping of a heptameric module in the nuclear pore complex. *J Cell Biol*. 196:419–434. doi:10.1083/jcb.201109008.

Feuerborn, A., and P.R. Cook. 2015. Why the activity of a gene depends on its neighbors. *Trends Genet*. 31:483–490. doi:10.1016/j.tig.2015.07.001.

Fischer, T., K. Sträßer, A. Rácz, S. Rodriguez-Navarro, M. Oppizzi, P. Ihrig, J. Lechner, and E. Hurt. 2002. The mRNA export machinery requires the novel Sac3p-Thp1p complex to dock at the nucleoplasmic entrance of the nuclear pores. *EMBO J*. 21:5843–5852. doi:10.1093/emboj/cdf590.

Freudenreich, C.H., and X.A. Su. 2016. Relocalization of DNA lesions to the nuclear pore complex. *FEMS Yeast Res*. 16:fow095. doi:10.1093/femsyr/fow095.

Fujimoto, M., R. Takii, and A. Nakai. 2023. Regulation of HSF1 transcriptional complexes under proteotoxic stress: mechanisms of heat shock gene transcription involve the stress-induced HSF1 complex formation, changes in chromatin states, and formation

of phase-separated condensates. *BioEssays*. 45:e2300036. doi:10.1002/bies.202300036.

Gallardo, P., P. Real-Calderón, I. Flor-Parra, S. Salas-Pino, and R.R. Daga. 2020. Acute heat stress leads to reversible aggregation of nuclear proteins into nucleolar rings in fission yeast. *Cell Rep*. 33:108377. doi:10.1016/j.celrep.2020.108377.

Galy, V., O. Gadal, M. Fromont-Racine, A. Romano, A. Jacquier, and U. Nehrbass. 2004. Nuclear retention of unspliced mRNAs in yeast is mediated by perinuclear Mlp1. *Cell*. 116:63–73. doi:10.1016/S0092-8674(03)01026-2.

Galy, V., J.C. Olivo-Marin, H. Scherthan, V. Doye, N. Rascalou, and U. Nehrbass. 2000. Nuclear pore complexes in the organization of silent telomeric chromatin. *Nature*. 403:108–112. doi:10.1038/47528.

Ge, T., D.G. Brickner, K. Zehr, D.J. VanBelzen, W. Zhang, C. Caffalette, S. Ungerleider, N. Marcou, B. Chait, M.P. Rout, and J.H. Brickner. 2024. Exportin-1 functions as an adaptor for transcription factor-mediated docking of chromatin at the nuclear pore complex. *bioRxiv {preprint]*. doi:10.1101/2024.05.09.593355.

Gomez-Pastor, R., E.T. Burchfiel, and D.J. Thiele. 2018. Regulation of heat shock transcription factors and their roles in physiology and disease. *Nat Rev Mol Cell Biol*. 19:4–19. doi:10.1038/nrm.2017.73.

Green, D.M., C.P. Johnson, H. Hagan, and A.H. Corbett. 2003. The C-terminal domain of myosin-like protein 1 (Mlp1p) is a docking site for heterogeneous nuclear ribonucleoproteins that are required for mRNA export. *Proc Natl Acad Sci U S A*. 100:1010–1015. doi:10.1073/pnas.0336594100.

Hakhverdyan, Z., K.R. Molloy, S. Keegan, T. Herricks, D.M. Lepore, M. Munson, R.I. Subbotin, D. Fenyö, J.D. Aitchison, J. Fernandez-Martinez, B.T. Chait, and M.P. Rout. 2021. Dissecting the structural dynamics of the nuclear pore complex. *Mol Cell*. 81:153-165.e7. doi:10.1016/j.molcel.2020.11.032.

Hampoelz, B., A. Andres-Pons, P. Kastritis, and M. Beck. 2019. Structure and assembly of the nuclear pore complex. *Annu Rev Biophys*. 48:515–536. doi:10.1146/annurev-biophys-052118-115308.

Heist, T., T. Fukaya, and M. Levine. 2019. Large distances separate coregulated genes in living Drosophila embryos. *Proc Natl Acad Sci U S A*. 116:15062–15067. doi:10.1073/pnas.1908962116.

Hentze, N., L. Le Breton, J. Wiesner, G. Kempf, and M.P. Mayer. 2016. Molecular mechanism of thermosensory function of human heat shock transcription factor Hsf1. *Elife*. 5:e11576. doi:10.7554/elife.11576.001.

Hnisz, D., K. Shrinivas, R.A. Young, A.K. Chakraborty, and P.A. Sharp. 2017. A phase separation model predicts key features of transcriptional control. *Cell*. 169:13–23. doi:10.1016/j.cell.2017.02.007.

Ibarra, A., C. Benner, S. Tyagi, J. Cool, and M.W. Hetzer. 2016. Nucleoporin-mediated regulation of cell identity genes. *Genes Dev*. 30:2253–2258. doi:10.1101/gad.287417.116.

Ishii, K., G. Arib, C. Lin, G. Van Houwe, and U.K. Laemmli. 2002. Chromatin boundaries in budding yeast: the nuclear pore connection. *Cell*. 109:551–562. doi:10.1016/S0092-8674(02)00756-0.

Jani, D., E. Valkov, and M. Stewart. 2014. Structural basis for binding the TREX2 complex to nuclear pores, GAL1 localisation and mRNA export. *Nucleic Acids Res*. 42:6686–6697. doi:10.1093/nar/gku252.

Kainth, A.S., S. Chowdhary, D. Pincus, and D.S. Gross. 2021. Primordial super-enhancers: heat shock-induced chromatin organization in yeast. *Trends Cell Biol*. 31:801–813. doi:10.1016/j.tcb.2021.04.004.

Kim, S., and D.S. Gross. 2013. Mediator recruitment to heat shock genes requires dual Hsf1 activation domains and Mediator tail subunits Med15 and Med16. *J Biol Chem*. 288:12197–12213. doi:10.1074/jbc.M112.449553.

Kim, S., I. Liachko, D.G. Brickner, K. Cook, W.S. Noble, J.H. Brickner, J. Shendure, and M.J. Dunham. 2017. The dynamic three-dimensional organization of the diploid yeast genome. *Elife*. 6:e23623. doi:10.7554/elife.23623.

Kosova, B., N. Panté, C. Rollenhagen, A. Podtelejnikov, M. Mann, U. Aebi, and E. Hurt. 2000. Mlp2p, a component of nuclear pore attached intranuclear filaments, associates with nic96p. *J Biol Chem*. 275:343–350. doi:10.1074/jbc.275.1.343.

Lee, J., L. Simpson, Y. Li, S. Becker, F. Zou, X. Zhang, and L. Bai. 2024. Transcription factor condensates, 3D clustering and gene expression enhancement of the MET regulon. *eLife.* 13:RP96028. doi:10.7554/elife.96028.3.

Levine, M., C. Cattoglio, and R. Tjian. 2014. Looping back to leap forward: transcription enters a new era. *Cell*. 157:13-25. doi:10.1016/j.cell.2014.02.009.

Li, Y., J. Lee, and L. Bai. 2024. DNA methylation-based high-resolution mapping of long-distance chromosomal interactions in nucleosome-depleted regions. *Nat Commun*. 15:4358. doi:10.1038/s41467-024-48718-y.

Light, W.H., D.G. Brickner, V.R. Brand, and J.H. Brickner. 2010. Interaction of a DNA zip code with the nuclear pore complex promotes H2A.Z incorporation and INO1 transcriptional memory. *Mol Cell*. 40:112–125. doi:10.1016/j.molcel.2010.09.007.

Lin, D.H., and A. Hoelz. 2019. The structure of the nuclear pore complex (an update). *Annu Rev Biochem*. 88:725–783. doi:10.1146/annurev-biochem-062917-011901.

Luthra, R., S.C. Kerr, M.T. Harreman, L.H. Apponi, M.B. Fasken, S. Ramineni, S. Chaurasia, S.R. Valentini, and A.H. Corbett. 2007. Actively transcribed GAL genes can be physically linked to the nuclear pore by the SAGA chromatin modifying complex. *J Biol Chem*. 282:3042–3049. doi:10.1074/jbc.m608741200.

Meeussen, J.V.W., W. Pomp, I. Brouwer, W.J. De Jonge, H.P. Patel, and T.L. Lenstra. 2023. Transcription factor clusters enable target search but do not contribute to target gene activation. *Nucleic Acids Res*. 51:5449-5468. doi:10.1093/nar/gkad227.

Mészáros, N., J. Cibulka, M.J. Mendiburo, A. Romanauska, M. Schneider, and A. Köhler. 2015. Nuclear pore basket proteins are tethered to the nuclear envelope and can regulate membrane curvature. *Dev Cell*. 33:285–298. doi:10.1016/j.devcel.2015.02.017.

Miné-Hattab, J., and I. Chiolo. 2020. Complex chromatin motions for DNA repair. *Front Genet*. 11:800. doi:10.3389/fgene.2020.00800.

Morawska, M., and H.D. Ulrich. 2013. An expanded tool kit for the auxin-inducible degron system in budding yeast. *Yeast*. 30:341–351. doi:10.1002/yea.2967.

Nair, S.J., L. Yang, D. Meluzzi, S. Oh, F. Yang, M.J. Friedman, S. Wang, T. Suter, I. Alshareedah, A. Gamliel, Q. Ma, J. Zhang, Y. Hu, Y. Tan, K.A. Ohgi, R.S. Jayani, P.R. Banerjee, A.K. Aggarwal, and M.G. Rosenfeld. 2019. Phase separation of

ligand-activated enhancers licenses cooperative chromosomal enhancer assembly. *Nat Struct Mol Biol*. 26:193–203. doi:10.1038/s41594-019-0190-5.

Niepel, M., K.R. Molloy, R. Williams, J.C. Farr, A.C. Meinema, N. Vecchietti, I.M. Cristea, B.T. Chait, M.P. Rout, and C. Strambio-De-Castillia. 2013. The nuclear basket proteins Mlp1p and Mlp2p are part of a dynamic interactome including Esc1p and the proteasome. *Mol Biol Cell*. 24:3920–3938. doi:10.1091/mbc.e13-07-0412.

Nishimura, K., T. Fukagawa, H. Takisawa, T. Kakimoto, and M. Kanemaki. 2009. An auxin-based degron system for the rapid depletion of proteins in nonplant cells. *Nature Methods* . 6:917–922. doi:10.1038/nmeth.1401.

O'Sullivan, J.M., S.M. Tan-Wong, A. Morillon, B. Lee, J. Coles, J. Mellor, and N.J. Proudfoot. 2004. Gene loops juxtapose promoters and terminators in yeast. *Nat Genet*. 36:1014–1018. doi:10.1038/ng.1411.

Palancade, B., X. Liu, M. Garcia-Rubio, A. Aguilera, X. Zhao, and V. Doye. 2007. Nucleoporins prevent DNA damage accumulation by modulating Ulp1-dependent sumoylation processes. *Mol Biol Cell*. 18:2912–2923. doi:10.1091/mbc.e07-02-0123.

Pincus, D., J. Anandhakumar, P. Thiru, M.J. Guertin, A.M. Erkine, and D.S. Gross. 2018. Genetic and epigenetic determinants establish a continuum of Hsf1 occupancy and activity across the yeast genome. *Mol Biol Cell*. 29:3168–3182. doi:10.1091/mbc.e18-06-0353.

Pliss, A., K. Malyavantham, S. Bhattacharya, M. Zeitz, and R. Berezney. 2009. Chromatin dynamics is correlated with replication timing. *Chromosoma*. 118:459–470. doi:10.1007/S00412-009-0208-6.

Powrie, E.A., D. Zenklusen, and R.H. Singer. 2011. A nucleoporin, Nup60p, affects the nuclear and cytoplasmic localization of ASH1 mRNA in S. cerevisiae. *RNA*. 17:134–144. doi:10.1261/rna.1210411.

Randise-Hinchliff, C., and J.H. Brickner. 2016. Transcription factors dynamically control the spatial organization of the yeast genome. *Nucleus*. 7:369–374. doi:10.1080/19491034.2016.1212797.

Regot, S., E. De Nadal, S. Rodriǵuez-Navarro, A. Gonzaĺez-Novo, J. Peŕez-Fernandez, O. Gadal, G. Seisenbacher, G. Ammerer, and F. Posas. 2013. The Hog1 stress-activated protein kinase targets nucleoporins to control mRNA export upon stress. *J Biol Chem*. 288:17384–17398. doi:10.1074/jbc.m112.444042.

Rohner, S., S.M. Gasser, and P. Meister. 2008. Modules for cloning-free chromatin tagging in Saccharomyces cerevisiae. *Yeast*. 25:235–239. doi:10.1002/yea.1580.

Rubio, L.S., and D.S. Gross. 2023. Dynamic coalescence of yeast heat shock protein genes bypasses the requirement for actin. *Genetics*. 223:iyad006. doi:10.1093/genetics/iyad006.

Rubio, L.S., S. Mohajan, and D.S. Gross. 2024. Heat shock factor 1 forms condensates and restructures the yeast genome before activating target genes. *Elife*. 12:RP92464. doi:10.7554/elife.92464.2.

Sabari, B.R., A. Dall'Agnese, A. Boija, I.A. Klein, E.L. Coffey, K. Shrinivas, B.J. Abraham, N.M. Hannett, A. V. Zamudio, J.C. Manteiga, C.H. Li, Y.E. Guo, D.S. Day, J. Schuijers, E. Vasile, S. Malik, D. Hnisz, T.I. Lee, I.I. Cisse, R.G. Roeder, P.A. Sharp, A.K. Chakraborty, and R.A. Young. 2018. Coactivator condensation at super-enhancers links phase separation and gene control. *Science*. 361:eaar3958. doi:10.1126/science.aar3958.

Sarma, N.J., T.M. Haley, K.E. Barbara, T.D. Buford, K.A. Willis, and G.M. Santangelo. 2007. Glucose-responsive regulators of gene expression in Saccharomyces cerevisiae function at the nuclear periphery via a reverse recruitment mechanism. *Genetics*. 175:1127–1135. doi:10.1534/genetics.106.068932.

Schindelin, J., I. Arganda-Carreras, E. Frise, V. Kaynig, M. Longair, T. Pietzsch, S. Preibisch, C. Rueden, S. Saalfeld, B. Schmid, J.Y. Tinevez, D.J. White, V. Hartenstein, K. Eliceiri, P. Tomancak, and A. Cardona. 2012. Fiji - an open source platform for biological image analysis. *Nat Methods*. 9:676–682. doi:10.1038/nmeth.2019.

Schmid, M., G. Arib, C. Laemmli, J. Nishikawa, T. Durussel, and U.K. Laemmli. 2006. Nup-PI: the nucleopore-promoter interaction of genes in yeast. *Mol Cell*. 21:379–391. doi:10.1016/j.molcel.2005.12.012.

Scholz, B.A., N. Sumida, C.D.M. de Lima, I. Chachoua, M. Martino, I. Tzelepis, A. Nikoshkov, H. Zhao, R. Mehmood, E.G. Sifakis, D. Bhartiya, A. Göndör, and R. Ohlsson. 2019. WNT signaling and AHCTF1 promote oncogenic MYC expression through super-enhancer-mediated gene gating. *Nat Genet*. 51:1723–1731. doi:10.1038/s41588-019-0535-3.

Sekinger, E.A., and D.S. Gross. 2001. Silenced chromatin is permissive to activator binding and PIC recruitment. *Cell*. 105:403–414. doi:10.1016/S0092-8674(01)00329-4.

Singh, D., N. Soni, J. Hutchings, I. Echeverria, F. Shaikh, M. Duquette, S. Suslov, Z. Li, T. Van Eeuwen, K. Molloy, Y. Shi, J. Wang, Q. Guo, B.T. Chait, J. Fernandez-Martinez, M.P. Rout, A. Sali, and E. Villa. 2024. The molecular architecture of the nuclear basket. *Cell*. 187:5267-5281.e13. doi:10.1016/j.cell.2024.07.020.

Sood, V., and J.H. Brickner. 2014. Nuclear pore interactions with the genome. *Curr Opin Genet Dev*. 25:43–49. doi:10.1016/j.gde.2013.11.018.

Sorger, P.K., and H.C.M. Nelson. 1989. Trimerization of a yeast transcriptional activator via a coiled-coil motif. *Cell*. 59:807–813. doi:10.1016/0092-8674(89)90604-1.

Strambio-de-Castillia, C., G. Blobel, and M.P. Rout. 1999. Proteins connecting the nuclear pore complex with the nuclear Interior. *J Cell Biol*. 144:839–855. doi:10.1083/jcb.144.5.839.

Taddei, A., G. Van Houwe, F. Hediger, V. Kalck, F. Cubizolles, H. Schober, and S.M. Gasser. 2006. Nuclear pore association confers optimal expression levels for an inducible yeast gene. *Nature*. 441:774–778. doi:10.1038/nature04845.

Taddei, A., H. Schober, and S.M. Gasser. 2010. The budding yeast nucleus. *Cold Spring Harb Perspect Biol*. 2:a000612. doi:10.1101/cshperspect.a000612.

Tan-Wong, S.M., H.D. Wijayatilake, and N.J. Proudfoot. 2009. Gene loops function to maintain transcriptional memory through interaction with the nuclear pore complex. *Genes Dev*. 23:2610–2624. doi:10.1101/gad.1823209.

Teixeira, M.T., S. Siniossoglou, S. Podtelejnikov, J. Claude Bénichou, M. Mann, B. Dujon, E. Hurt, and E. Fabre. 1997. Two functionally distinct domains generated by invivo cleavage of Nup145p: a novel biogenesis pathway for nucleoporins. *EMBO J*. 16:5086–5097. doi:10.1093/emboj/16.16.5086ï.

Tyagi, S., J.S. Capitanio, J. Xu, F. Chen, R. Sharma, J. Huang, and M.W. Hetzer. 2023. High-precision mapping of nuclear pore-chromatin interactions reveals new principles

of genome organization at the nuclear envelope. *eLlife.* 12:RP87462. doi:10.7554/elife.87462.1.

Venturi, C.B., A.M. Erkine, and D.S. Gross. 2000. Cell cycle-dependent binding of yeast heat shock factor to nucleosomes. *Mol Cell Biol*. 20:6435–6448. doi:10.1128/mcb.20.17.6435-6448.2000.

Verghese, J., J. Abrams, Y. Wang, and K.A. Morano. 2012. Biology of the heat shock response and protein chaperones: budding Yeast (Saccharomyces cerevisiae) as a model system. *Microbiol Mol Biol Rev*. 76:115–158. doi:10.1128/mmbr.05018-11.

Vinciguerra, P., N. Iglesias, J. Camblong, D. Zenklusen, and F. Stutz. 2005. Perinuclear Mlp proteins downregulate gene expression in response to a defect in mRNA export. *EMBO J*. 24:813–823. doi:10.1038/sj.emboj.7600527.

Wente, S.R., and G. Blobel. 1994. NUP145 encodes a novel yeast glycine-leucine-phenylalanine-glycine (GLFG) nucleoporin required for nuclear envelope structure. *J Cell Biol*. 125:955–969. doi:10.1083/jcb.125.5.955.

Zhang, H., S. Shao, Y. Zeng, X. Wang, Y. Qin, Q. Ren, S. Xiang, Y. Wang, J. Xiao, and Y. Sun. 2022. Reversible phase separation of HSF1 is required for an acute transcriptional response during heat shock. *Nat Cell Biol*. 24:340–352. doi:10.1038/s41556-022-00846-7.

Zhao, J., J. Herrera-Diaz, and D.S. Gross. 2005. Domain-wide displacement of histones by activated heat shock factor occurs independently of Swi/Snf and is not correlated with RNA polymerase II density. *Mol Cell Biol*. 25:8985–8999. doi:10.1128/mcb.25.20.8985-8999.2005.

Zhu, X., C. Qi, R. Wang, J.H. Lee, J. Shao, L. Bei, F. Xiong, P.T. Nguyen, G. Li, J. Krakowiak, S.P. Koh, L.M. Simon, L. Han, T.I. Moore, and W. Li. 2022. Acute depletion of human core nucleoporin reveals direct roles in transcription control but dispensability for 3D genome organization. *Cell Rep*. 41:111576. doi:10.1016/j.celrep.2022.111576.

Zsok, J., F. Simon, G. Bayrak, L. Isaki, N. Kerff, Y. Kicheva, A. Wolstenholme, L.E. Weiss, and E. Dultz. 2024. Nuclear basket proteins regulate the distribution and mobility of nuclear pore complexes in budding yeast. *Mol Biol Cell*. 35:ar143. doi:10.1091/mbc.e24-08-0371.

Table 1

Role of NPC proteins

Features	Nup2	Mlp1	Nup1	Nup145	References
FG repeats	Yes	No	Yes	Yes (Nup145N) No (Nup145C)	(Denning et al., 2003; Dekker et al., 2023; Aitchison and Rout, 2012)
Phase separation propensity	Yes (PSP score 0.9453)	Yes (PSP score 0.8533)	Yes (PSP score 0.9772)	Yes (PSP score 0.7217)	PSPredictor
Nonessential/ Essential	Non-essential	Non-essential	Essential	Essential	SGD (yeastgenome.org)
mRNA export	Yes /Mild	Yes /Mild	Yes	Yes	(Regot et al., 2013; Powrie et al., 2011; Green et al., 2003; Galy et al., 2004; Vinciguerra et al., 2005; Bensidoun et al., 2022; Fischer et al., 2002; Jani et al., 2014; Fabre et al., 1994; Dockendorff et al., 1997)
mRNA quality control	?	Yes	?	?	(Galy et al., 2004; Fasken et al., 2008)
NPC and NE integrity	?	?	Yes	Yes	(Mészáros et al., 2015; Dockendorff et al., 1997; Wente and Blobel, 1994)
NPC components	NPC Basket	NPC Basket filament	Connector of NPC basket to NPC and NE	Nup145C-Scaffold of NPC, Nup145N-NPC central core	(Singh et al., 2024; Lin and Hoelz, 2019; Hakhverdyan et al., 2021; Dilworth et al., 2001; Niepel et al., 2013; Strambio-de-Castillia et al., 1999; Mészáros et al., 2015; Alber et al., 2007).
Dynamic /stable	Dynamic	Dynamic	Dynamic	Nup145N-Dynamic Nup145-Very slow exchange	(Hakhverdyan et al., 2021; Dilworth et al., 2001; Denoth-Lippuner et al., 2014; Niepel et al., 2013).
Insulator/boundary activity	Yes	?	?	?	(Dilworth et al., 2005; Ishii et al., 2002)

Role in repositioning of inducible genes to NPC	Yes (*SSA2, SSA4, HIS4; GAL1-10*; *INO1, HAS1-TDAI*	Yes (Mating response genes, *HXK1; GAL1-10*, *HSP104*)	Yes (*INO1, GAL10*)	Yes *SUC2*	(Brickner et al., 2019; Schmid et al., 2006; Ahmed et al., 2010; Brickner et al., 2007; Light et al., 2010; Kim et al., 2017; Casolari et al., 2005; Tan-Wong et al., 2009; Dieppois et al., 2006; Casolari et al., 2004; Cabal et al., 2006; Brickner et al., 2016; Jani et al., 2014; Brickner and Brickner, 2010; Sarma et al., 2007).
Chromatin association (ChIP, IF, CHEC)	Yes (*GAL* genes, *HXK1, INO1*)	Yes (*GAL2, GAL1-10), HXK1, INO1)*	?	Yes (*SUC2)* (Nup145C)	(Brickner et al., 2019; Ahmed et al., 2010; Brickner et al., 2007; Light et al., 2010; Casolari et al., 2004; Sarma et al., 2007; Schmid et al., 2006; Brickner et al., 2012; Luthra et al., 2007; Tan-Wong et al., 2009).

Abbreviations

3C	Chromosome Conformation Capture
AID	Auxin Inducible Degradation
ChIP	Chromatin Immunoprecipitation
CHEC	Chromatin Endogenous Cleavage
ConA	Concanavalin A
3D	Three Dimensional
FG	Phenylalanine-Glycine
FxFG	Phenylalanine-any amino acid-Phenylalanine-Glycine
GFP	Green Fluorescence Protein
GRS	Gene Recruitment Sequence
HS	Heat Shock
NHS	Non-Heat Shock
Hsf1	Heat Shock Factor 1
HSE	Heat Shock Element
HSP	Heat Shock Protein
HSR	Heat Shock Response
HGC	*HSR* Gene Coalescence
IAA	Indole Acetic Acid
IF	Immunofluorescence
mNG	mNeonGreen
NE	Nuclear Envelope
NPC	Nuclear Pore Complex
NB	Nuclear Basket
Nup	Nucleoporin
O/N	Overnight
RT-qPCR	Reverse Transcription-quantitative PCR
SE	Super Enhancer
TF	Transcription Factor
UAS	Upstream Activating Sequence
UTR	Untranslated Region
YFP	Yellow Fluorescence Protein